



Applied Catalysis B: Environmental

journal homepage: www.elsevier.com/locate/apcatb

Review

Doping of graphitic carbon nitride for photocatalysis: A review



Longbo Jiang^{a,b}, Xingzhong Yuan^{a,b,*}, Yang Pan^{a,b}, Jie Liang^{a,b}, Guangming Zeng^{a,b},
Zhibin Wu^{a,b}, Hou Wang^{a,b,c,**}

^a College of Environmental Science and Engineering, Hunan University, Changsha 410082, PR China

^b Key Laboratory of Environmental Biology and Pollution Control (Hunan University), Ministry of Education, Changsha 410082, PR China

^c School of Chemical and Biomedical Engineering, Nanyang Technological University, Singapore 637459, Singapore

ARTICLE INFO

Article history:

Received 18 April 2017

Received in revised form 31 May 2017

Accepted 3 June 2017

Available online 10 June 2017

Keywords:

$g\text{-C}_3\text{N}_4$

Element doping

Visible light photocatalysis

Band gap engineering

Heterojunction

ABSTRACT

As a fascinating conjugated polymer, graphitic carbon nitride ($g\text{-C}_3\text{N}_4$) has been the hotspot in the materials science as a metal-free and visible-light-responsive photocatalyst. Pure $g\text{-C}_3\text{N}_4$ suffers from the insufficient sunlight absorption, low surface area and the fast recombination of photo-induced electron-hole pairs, resulting in low photocatalytic activity. Element doping is known to be an efficient method to tune the unique electronic structure and band gap of $g\text{-C}_3\text{N}_4$, which considerably broaden the light responsive range and enhance the charge separation. This review summarizes the recent progress in the development of efficient and low cost doped $g\text{-C}_3\text{N}_4$ systems in various realms such as photocatalytic hydrogen evolution, reduction of carbon dioxide, photocatalytic removal of contaminants in wastewater and gas phase. Typically, metal doping, nonmetal doping, co-doping and heterojunction based on doped $g\text{-C}_3\text{N}_4$ have been explored to simultaneously tune the crystallographic, textural and electronic structures for improving photocatalytic activity by enhancing the light absorption, facilitating the charge separation and transportation and prolonging the charge carrier lifetime. Finally, the current challenges and the crucial issues of element doped $g\text{-C}_3\text{N}_4$ photocatalysts that need to be addressed in future research are presented. This review presented herein can pave a novel avenue and add invaluable knowledge to the family of element doped $g\text{-C}_3\text{N}_4$ for the develop of more effective visible-light-driven photocatalysts.

© 2017 Elsevier B.V. All rights reserved.

Contents

1. Introduction	389
2. Metal doping.....	389
2.1. Alkali metal	389
2.2. Transition metal	391
3. Non-metal doping	392
3.1. Phosphorus doping	392
3.2. Sulfur doping.....	395
3.3. Oxygen doping	396
3.4. Carbon, nitrogen or boron doping	398
3.5. Halogen doping	399
4. Co-doping.....	401
5. Heterojunction based on doped $g\text{-C}_3\text{N}_4$	401

* Corresponding author at: College of Environmental Science and Engineering, Hunan University, Changsha 410082, PR China.

** Corresponding author at: Key Laboratory of Environmental Biology and Pollution Control (Hunan University), Ministry of Education, Changsha 410082, PR China.

E-mail addresses: yxz@hnu.edu.cn (X. Yuan), hankewanghou024@163.com (H. Wang).

6. Conclusion and perspectives	403
Acknowledgements	403
References	403

1. Introduction

The increasing global crisis of energy shortage and environmental issues are becoming serious threats to the sustainable development of human society. With outstanding merits including environmentally friendly and inexhaustible supply, sunlight has been served as the most ideal power to resolve the energy shortage and pollution removal. Particularly, semiconductor-based photocatalysis has been considered as an renewable, economic, safe, and clean technology, which conduct catalytic reactions for a variety of applications, such as water splitting [1–5], reduction of CO₂ [6–10], removal of organic pollutants [11–19], bacteria disinfection [20–22], and selective synthesis of organic compounds [23–26]. Nevertheless, the low solar-energy utilization efficiency and the wide band gap still remain the “bottleneck” of the photocatalysts to satisfy the requirements of practical applications [27]. For example, TiO₂ has become the most popular and widely used photocatalyst since Fujishima and Honda found that water can be split into hydrogen by using TiO₂ as photoanode in 1972 [28]. However, due to the fact that TiO₂ has broad bandgaps (~3.2 eV), the use of TiO₂ is limited by its poor performances under visible light irradiation. In order to achieve the practical use of photocatalysts and overcome the drawbacks of wide bandgap TiO₂, various modified TiO₂ and TiO₂-alternative photocatalysts with narrow bandgap, have been developed to efficiently utilize the visible light in solar light [29–34]. Currently, it is still a challenge to develop novel photocatalysts that are stable, abundant, efficient and facile in fabrication.

Recently, two-dimensional (2D) materials, graphene, graphitic carbon nitride (g-C₃N₄), transition-metal dichalcogenides, and hexagonal boron nitride with excellent properties have been widely used in optical and electronic devices, chemical sensors, energy generation and storage, as well as environmental remediation [35–42]. Particularly, g-C₃N₄ has attracted intensive attention for its promising applications in photochemistry and photocatalysis as a metal-free polymer semiconductor with tri-s-triazine units [39,43,44]. In detail, g-C₃N₄ is a medium band gap semiconductor with good visible light response (up to 460 nm). This suitable band gap, together with low cost, facile in preparation, high chemical stability, and pollution-free feature, is especially suitable for applications in photocatalytic organic pollutant degradation, water splitting, CO₂ reduction and organic synthesis under visible light [27,36,45–47]. However, the pristine g-C₃N₄ is usually restricted by unsatisfactory photocatalytic efficiency due to the insufficient solar light absorption, low surface area and the fast recombination of photogenerated electron-hole pairs [39,48]. Generally, each photocatalytic reaction would involve three processes: photon absorption, electron–hole charges generation and separation, and catalytic surface reactions [49]. Therefore, various modification strategies, such as elemental and molecular doping [50,51], preparation of mesoporous g-C₃N₄ [52], exfoliation to two-dimensional (2D) nanosheets [53], combination with conductive materials [54,55], nanocomposite structure construction with other semiconductors [43] and dye sensitization [56] are adopted to enhance the photocatalytic activity of g-C₃N₄.

It is well known that g-C₃N₄ owns tunable band gap with controllable lowest unoccupied molecular orbital (LUMO) and highest occupied molecular orbital (HOMO) [57]. It can remarkably affect the photoelectronic performance of g-C₃N₄ as a functional photocatalytic nanosheet. Meanwhile, The tunable band gap of g-C₃N₄

simplifies the modification process mainly by element doping or heterojunctions structure construction [57]. Significantly, doping, that is designed by deliberately introducing impurities, is known to be an efficient method to tune the band gap of g-C₃N₄, which considerably broaden the light absorption and accelerate the electron–hole pairs separation. Doping of g-C₃N₄ with P, S, C, I, or B via either interstitial or substitutional doping has been applied to modify its texture and electronic structure for enhancing the photocatalytic activity [58–62]. Also, alkali metals and transitional metals (K, Na, Fe, Cu, and W) have been incorporated into the framework of g-C₃N₄ to enhance the photocatalytic performance [63–66]. Orbital hybridization occurs between the dopant orbital and the molecular orbital of g-C₃N₄, leading to a tunable electronic structure and potentials of valence band (VB) and conduction band (CB) [63,67].

Recently, the field of research and development of element doped g-C₃N₄ photocatalysts is currently undergoing an exciting development with increasing achievements. In spite of several excellent reviews focusing on the synthesis and modification of g-C₃N₄-based photocatalysts and their applications in solving the energy and environmental issues [27,48,68–70]. However, only a handful of reviews have focused on the versatile properties and rational design of g-C₃N₄-based photocatalysts by doping. Element doping is considered as an efficient strategy to distinctly tune the optical, electronic, luminescent and other physical properties of g-C₃N₄. In the field of photocatalysis, band gap engineering of g-C₃N₄ via the incorporation of cations, anions, or the codoping of both plays an excellent role to modulate the light absorption and redox band potentials for targeted photocatalytic applications. Thus, we believe that a comprehensive review on this subject is necessary to accelerate further developments. In this review, we intend to summarize the recent progress in the development of efficient and low cost doped g-C₃N₄ systems in various realms such as photocatalytic hydrogen evolution, reduction of carbon dioxide, photocatalytic removal of contaminants in wastewater and gas phase. Finally, the current challenges and the crucial issues of element doped g-C₃N₄ photocatalysts that need to be addressed in future research are presented.

2. Metal doping

Generally, the introduction of metallic impurities inflicts additional binding functions, which endows the doped system with unique photocatalytic properties by lowering the band gap and enhancing the absorption of visible light [63,64,71,72]. Table 1 summarizes metal-doped g-C₃N₄ photocatalysts and their physiochemical properties, as well as photocatalytic performances. In order to import metal ions into the framework of carbon nitrides, the corresponding soluble salt is always uniformly mixed with the precursor of g-C₃N₄. In this way, metallic impurities will be simultaneously doped into the g-C₃N₄ framework during the thermal condensation process of precursor.

2.1. Alkali metal

Alkali-metal ions such as K⁺ and Na⁺ were coordinated into the nitrogen pots of g-C₃N₄ framework, which could remarkably ameliorate the transfer, transport and separation efficiency of charge carriers to induce a spatial charge-carrier distribution for enhanced photocatalytic redox reactions [63,73]. Hu et al. first prepared band gap-tunable potassium doped g-C₃N₄ using dicyandiamide and

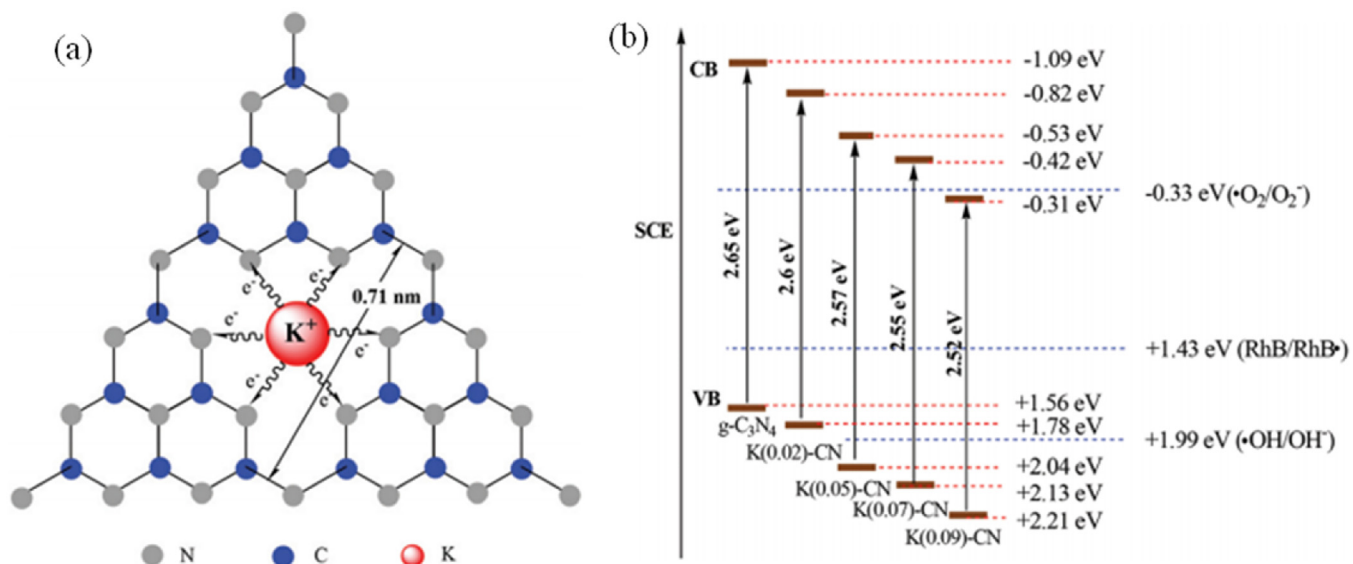


Fig. 1. (a) Possible doping site for K ions in K(x)-CN; (b) Band gap structures of as-prepared g-C₃N₄ and K(x)-CN. Reprinted with permission from ref. [67] Copyright 2015 Royal Society of Chemistry.

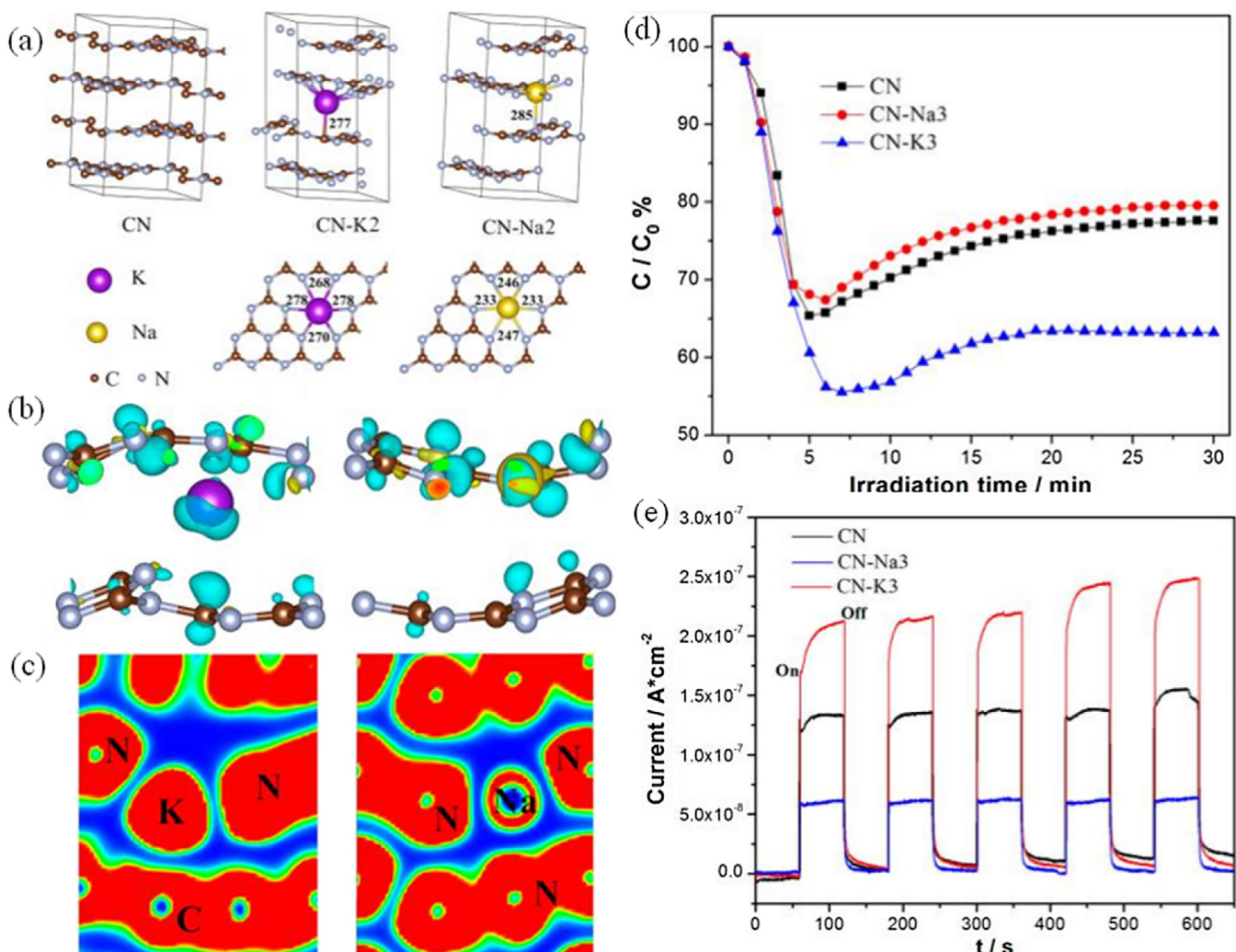


Fig. 2. Calculated crystal structures of CN, CN-K2 and CN-Na2 (a); Charge difference distribution of CN-K2 (left) and CN-Na2 (right) (b); electronic location function (ELF) analysis of CN-K2 and CN-Na2 (c); Comparison of the visible-light photocatalytic activity of CN, CN-Na3, and CN-K3 (d); Transient photocurrent responses of CN, CN-Na3, and CN-K3 (e). Reprinted with permission from ref. [63] Copyright 2016 American Chemical Society.

Table 1
Metal-doped g-C₃N₄ and their properties.

Doping element	Precursor	Synthesis	E _g (eV)	Application	Enhanced photocatalytic activity/pristine	Modified surface area/pristine, m ² g ⁻¹	Reference
K	KOH (K) Dicyandiamide (CN)	Annealing	2.57	RhB degradation	0.011 min ⁻¹ /0.0017 min ⁻¹ (6.4 times)	26.9/8.9	[67]
Na	NaOH (Na) Dicyandiamide (CN)	Thermal polymerization	2.58	RhB degradation	0.0064 min ⁻¹ /0.0018 min ⁻¹ (3.6 times)	29.6/8.9	[74]
K	KI (K) Dicyandiamide (CN)	Thermal polymerization	2.64	Phenol degradation	0.036 min ⁻¹ /0.011 min ⁻¹ (3.3 times)	-/-	[73]
K	KBr (K) Thiourea (CN)	Thermal polymerization	2.15	NO removal	0.1061 min ⁻¹ /0.0939 min ⁻¹ (1.1 times)	11/27	[63]
Fe	Ferric chloride (Fe) Melamine (CN)	Impregnation	2.56	RhB degradation	4.5 times higher than pure g-C ₃ N ₄ nanosheets	365.78/358.22	[64]
Fe	Fe(NO ₃) ₃ 9H ₂ O (Fe) Melamine (CN)	Thermal condensation	2.64	RhB degradation	99.5% degradation/68.5% degradation (2 h)	-/-	[86]
Cu	CuCl ₂ (Cu) Melamine (CN)	Thermal condensation	-	MB degradation	100% degradation/42% degradation (15 min)	40.86/5.26	[87]
Cu	CuCl ₂ (Cu) Melamine (CN)	Thermal condensation	2.25	MO degradation	90.2% degradation/19.7% degradation (1 h)	80.5/34.8	[80]
Ce	Ce(SO ₄) ₂ 4H ₂ O(Ce) Melamine (CN)	Annealing	2.57	RhB degradation	0.0155 min ⁻¹ /0.0073 min ⁻¹ (2.1 times)	18.8/11.1	[88]
Co	CoPc (Co) Melamine (CN)	Thermal condensation	2.62	H ₂ evolution	28 μmol·h ⁻¹ /9.5 μmol·h ⁻¹ (3 times)	33.1/13.2	[89]
Eu	Eu(NO ₃) ₃ (Eu) Melamine (CN)	Thermal condensation	2.41	MB degradation	0.0121 min ⁻¹ /0.0058 min ⁻¹ (2.1 times)	23/12	[90]
Mo	(NH ₄) ₆ Mo ₇ O ₂₄ 4H ₂ O (Mo) Melamine (CN)	Thermal condensation	1.45	CO ₂ reduction	CO yield 887 μmol g ⁻¹ CH ₄ yield 123 μmol g ⁻¹	88.21/13.52	[82]
W	Na ₂ WO ₄ (W) Urea, Dicyandiamide (CN)	Hydrothermal	-	MO degradation	0.0627 min ⁻¹ /0.0213 min ⁻¹ (3.12 times)	34.5/6.3	[91]
Y	Yttrium nitrate (Y) Urea (CN)	Thermal condensation	2.50	RhB degradation	100% degradation (110 min)	103/68	[77]
Zr	Zirconium nitrate (Zr) Urea (CN)	Thermal condensation	2.55	RhB degradation	100% degradation/70% degradation (110 min)	144.5/66.2	[75]

potassium hydrate as precursors [67]. As shown in Fig. 1a, the ions of K might be coordinated to the big C–N rings. Furthermore, they found that the CB and VB potentials of g-C₃N₄ could be tuned by changing the K concentration (as depicted in Fig. 1b). Thus, both •OH and •O₂[–] could be formed, leading to much higher photodegradation rate. At the same time, Zhang et al. synthesized Na doped g-C₃N₄ photocatalyst with a tunable band gap using dicyandiamide and sodium hydrate as precursors [74]. The similar results were obtained after Na doping on g-C₃N₄ photocatalyst. The CB and VB potentials could be tuned by controlling the sodium concentration. However, as shown in Table 1, the RhB degradation rate was lower than K doped g-C₃N₄ at the same condition. This indicated that although the effects of K doping and Na doping on g-C₃N₄ were similar, the K doping was more suitable for enhancing the photocatalytic activity [67,74]. Recently, Xiong et al. further studied the position of the introduced K and Na atoms and the essential evidence for the different photocatalytic performance [63]. Through the DFT calculations, they found that the bandgap of g-C₃N₄ could be narrowed by both K and Na doping, but they exerted a different impact on the electronic structure and photocatalytic performance of g-C₃N₄. As depicted in Fig. 2a, K atoms, tended to exist in the g-C₃N₄ interlayer via bridging the layers, while Na atoms were doped into the conjugated plane. Meanwhile, K atoms could chemically bond with atoms at the adjacent two layers which benefit to forming charge delivery channels and bridging the layers, contributing to the transfer and separation of photogenerated electron-hole pairs (Fig. 2b). However, Na atoms combine with in-planar N atoms with ionic bonds due to the loss of the 3 s electrons (Fig. 2c). As can be seen in Fig. 2d, CN-K3 shows higher photocatalytic activity for photocatalytic removal of NO than pure g-C₃N₄. Furthermore, CN-K3 displays an improved photocurrent when compared with CN, but CN-Na3 shows a decreased photocurrent (Fig. 2e). The K doping of g-C₃N₄ would result in increased visible-light absorption, suppressed recombination of charge pairs, and strong oxidation

capability, benefiting from extended π conjugated systems, narrowed band gap and positive-shifted valence band position.

2.2. Transition metal

Apart from the alkali-metal doping, other metal doping such as Pd, Fe, Cu, W, Zr, and so forth has also been broadly applied to modify the optical and electronic properties of g-C₃N₄ [64–66,75,76]. Metal doping can efficiently increase the light absorption, reduce the band gap, accelerate the charge mobility, and prolong the lifetime of charge carriers, which are all necessary for pronounced photocatalytic activity [36,77]. In fact, g-C₃N₄ can easily capture the metal cations due to the strong interactions between the cations and the negatively charged nitrogen atoms ascribed to lone pairs of electrons in the nitrogen pots of g-C₃N₄ [36,78].

Noble metal, such as Pt and Pd, were used to functionalize the g-C₃N₄ with improved carrier mobility, enhanced electron-hole separation, and narrowed band gap [79]. Pan et al. proposed and designed novel g-C₃N₄-based nanotubes based on the first-principles calculations [79]. They found that the electronic and optical properties of g-C₃N₄ can be easily optimized by functionalization with metal atoms (Pt and Pd). The optimized geometry and the calculated PDOS of Pt-d electrons and Pd-d electrons, together with calculated loss functions and calculated absorption spectra of g-C₃N₄-zz4 with and without functionalization were demonstrated in Fig. 3. These calculated results indicated that metal-functionalized would enhance the mobility, narrow the bandgap and optical gap, promote the enhanced absorption and photocatalytic activity in the visible-light region. Although noble metal doping can improve the photocatalysis activity of g-C₃N₄, the high price impedes its practical application. Researchers have focused on other transition metal, such as Fe, Cu, W, Zn, Mo, Zr, etc [64,66,75,80–84]. For example, Tonda et al. synthesis Fe-doped g-C₃N₄ nanosheets by a facile and cost effective method. They found

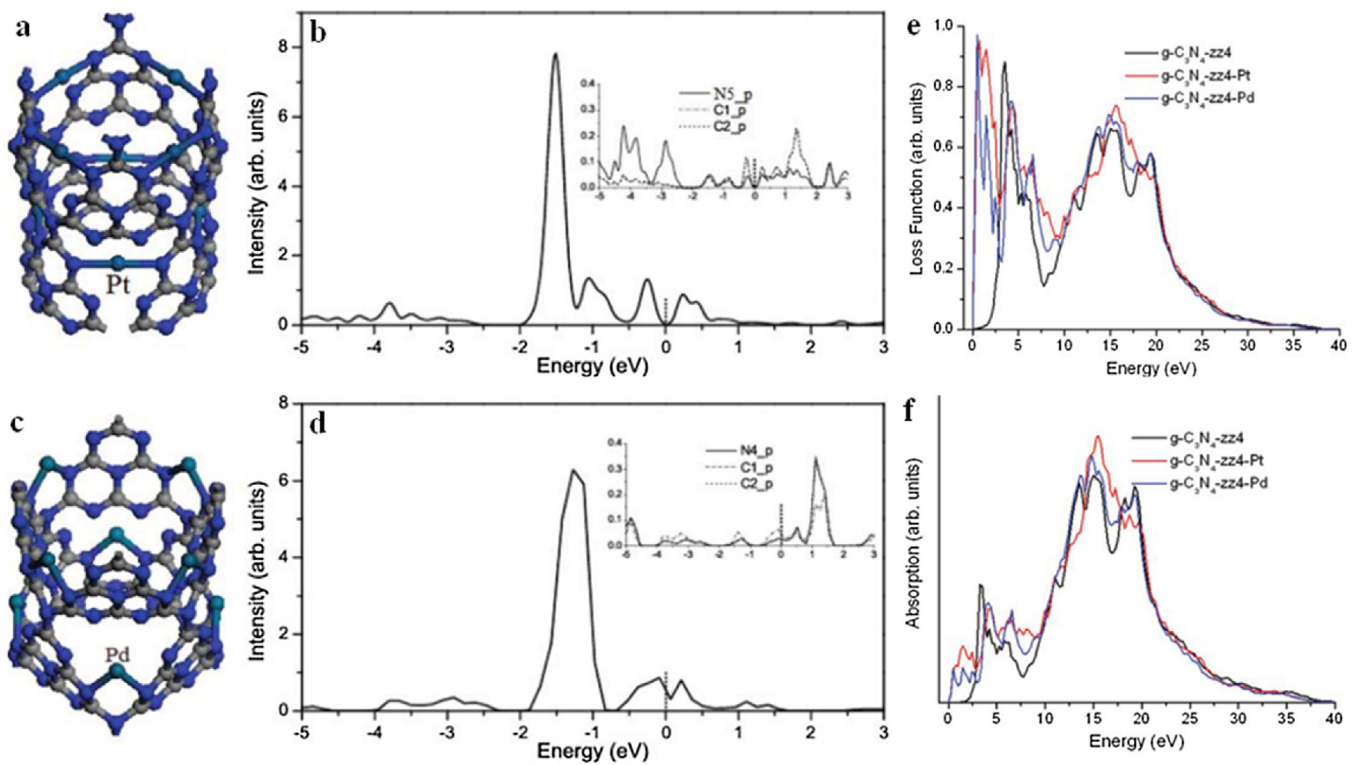


Fig. 3. Optimized geometry (a, c) and the calculated PDOS of Pt-d electrons (b) and Pt-d electrons (d) of Pt-functionalized $\text{g-C}_3\text{N}_4$ -zz4 and Pd-functionalized $\text{g-C}_3\text{N}_4$ -zz4; Calculated loss functions (e) and calculated absorption spectra (f) of $\text{g-C}_3\text{N}_4$ -zz4 with and without functionalization. Reprinted with permission from ref. [79] Copyright 2011 American Chemical Society.

that Fe doping had a great impact on the electronic and optical properties of $\text{g-C}_3\text{N}_4$ nanosheets. The obtained Fe-doped $\text{g-C}_3\text{N}_4$ nanosheets exhibit red shift and increased absorption in the visible light range. The Fe species were determined to be in the +3 oxidation state which can act as a temporary photogenerated electron and hole trapping site. These trapped electrons can reduce O_2 to O_2^- . Meanwhile, valance holes can oxidize OH^- or H_2O molecules to •OH using Fe^{3+} as a mediator. Therefore, the photocatalytic activity was much enhanced for RhB degradation. Afterwards, Li et al. prepared Fe-Doped $\text{g-C}_3\text{N}_4$ through a facile thermal method and employed for water splitting with enhanced photocatalytic H_2 production [65]. Molybdenum doped $\text{g-C}_3\text{N}_4$ catalysts were prepared by a simple pyrolysis method using common precursors [82]. They found that the introduction of Mo species can effectively reduce the recombination rate of photogenerated charges, enlarge the surface area, extend the visible light response, obtain mesoporous structure and narrow band gap energy. Therefore, Mo-doped $\text{g-C}_3\text{N}_4$ catalysts exhibited considerably higher activity for CO_2 reduction. Rare earth elements, yttrium, was also applied to dope on $\text{g-C}_3\text{N}_4$ for enhanced RhB degradation by a facile pyrolysis method with urea used as a precursor and yttrium nitrate as the Y source [77].

In short, metal ions were extensively applied as dopants for $\text{g-C}_3\text{N}_4$. Generally, the introduction of metal ions can result in the formation of new energy levels in the band-gap, extend the visible light response, and can sometimes suppress the recombination rate of the electron–hole charges. Although many studies on alkali-metal or transition metal-doped $\text{g-C}_3\text{N}_4$ have been reported, some disadvantages of metal doping have been found. For example, the thermal stability of the doped ions is poor. Furthermore, the newly created energy bands might act as recombination centres, leading to decreased quantum efficiencies [85].

3. Non-metal doping

In order to keep the metal-free property of $\text{g-C}_3\text{N}_4$, non-metal doping has attracted intensive attention. Moreover, non-metals always own high ionization energies and high electro negativity. Thus, non-metals can usually form covalent bonds by gaining electrons when reacting with other compounds. Meanwhile, non-metal doping can also avoid the thermal variation of chemical states of doped metal ions. As shown in Table 2, various non-metal dopants including phosphorus [9,50,92,93], sulphur [94–97], carbon [60,98], nitrogen [99], oxygen [100–102], boron [62,103], and halogen [104–106] have been employed for doping on $\text{g-C}_3\text{N}_4$.

3.1. Phosphorus doping

Phosphorus-doped $\text{g-C}_3\text{N}_4$ was first synthesized by a facile poly-condensation of a mixture with dicyandiamide as $\text{g-C}_3\text{N}_4$ precursor and a phosphorus-containing ionic liquid, i.e., 1-butyl-3-methylimidazolium hexafluorophosphate (BmimPF_6) [107]. With the increase of temperature, PF_6^- would react with amine groups, leading to join into the C–N framework. FT-IR, XPS and NMR results revealed that the phosphorus heteratoms most probably substitute the corner or bay carbon in the structure to form P–N bonding in C_3N_4 framework. They found that doping with a lower percentage of P heteratoms could remarkably change the electronic structure of $\text{g-C}_3\text{N}_4$, lower the optical band gap energy, and increase the electric conductivity. They further predicted that P doped $\text{g-C}_3\text{N}_4$ could be suitable for the photovoltaic applications. After that, Zhang et al. prepared the P doped $\text{g-C}_3\text{N}_4$ using the same raw material, which exhibited obvious enhanced photocatalytic activities for RhB and MO degradation [108]. It is known that the P doping site is influenced by the phosphorus source, which can

Table 2
Nonmetal-doped g-C₃N₄ and their properties.

Doping element	Precursor	Synthesis	E _g (eV)	E _{CB} (eV)	E _{VB} (eV)	Application	Enhanced activity/pristine	Light absorption	Charge separation	Modified surface area/pristine, m ² g ⁻¹	Reference
P	(NH ₄) ₂ HPO ₄ (P) Dicyandiamide (CN)	Co-polycondensation	2.63	–	–	RhB degradation	0.0466 min ⁻¹ / 0.0115 min ⁻¹ (4 times)	Improved	Enhanced	16.9/10.9	[109]
P	NH ₄ PF ₆ (P) NH ₄ SCN(CN)	Co-polycondensation	2.86	–0.99	1.87	RhB degradation	0.09856 min ⁻¹ / 0.03679 min ⁻¹ (2.7 times)	Improved	Enhanced	–	[112]
P	BmimPF ₆ (P) Dicyandiamide (CN)	Co-polycondensation	–	–	–	RhB degradation	98% degradation/ 58.2% degradation (1 h)	Improved	Enhanced	15/10	[108]
P	Diphosphonic acid (P) Melamine (CN)	Co-polycondensation	–	–	–	H ₂ evolution	104.1 μmol h ⁻¹ / 11.2 μmol h ⁻¹ (9.3 times)	Improved	Enhanced	83/7	[111]
P	2-aminoethylphosphonic acid(P) Melamine (CN)	Co-polycondensation	2.91	–0.83	2.08	H ₂ evolution	1596 μmol h ⁻¹ g ⁻¹ / 108 μmol h ⁻¹ g ⁻¹ (14.8 times)	Improved	Enhanced	122.6/5.6	[92]
P	Hexachlorocyclo-triphosphazene(P) Guanidiniumhydrochloride (CN)	Co-polycondensation	2.71	–0.59	2.12	H ₂ evolution	50.6 μmol h ⁻¹ / 17.45 μmol h ⁻¹ (2.9 times)	Decreased	Enhanced	32.8/26.86	[50]
P	phosphorous acid (P) Melamine (CN)	Hydrothermal treatment	2.55	–1.11	1.44	H ₂ evolution	67 μmol h ⁻¹ / 9 μmol h ⁻¹ (7.4 times)	Improved	Enhanced	22.95/3.73	[93]
S	H ₂ S (g) (S) Dicyandiamide (CN)	Heating-treated in H ₂ S	2.85	–1.06	1.79	H ₂ evolution	8.0 times (under λ > 400 nm)	–	–	63/12	[94]
S	Thiourea (S) Cyanamide (CN)	Co-polycondensation	2.82	–1.13	1.69	H ₂ evolution	12.16 μmol h ⁻¹ / 2.03 μmol h ⁻¹ (6.0 times)	Improved	Enhanced	–	[131]
S	Tri-thiocyanuric acid (S) Melamine (CN)	Co-polycondensation	–	–	–	H ₂ evolution	5000 μmol h ⁻¹ g ⁻¹ / 538 μmol h ⁻¹ g ⁻¹ (9.3 times)	Improved	–	28/6	[121]
S	Thiourea (S and CN)	Polycondensation	2.63	–	–	CO ₂ reduction	1.12 μmol g ⁻¹ / 0.81 μmol g ⁻¹ (1.38 times)	Improved	Enhanced	4.4/8.0	[95]
S	Tri-thiocyanuric acid (S) Melamine (CN)	Co-polycondensation	2.56	–	–	RhB degradation	0.0167 min ⁻¹ / 0.0013 min ⁻¹ (12.8 times)	Improved	Enhanced	52/15	[119]
S	Thiourea (S and CN)	Polycondensation	2.38	–1.28	1.10	UO ₂ ²⁺ reduction	0.13 min ⁻¹ / 0.07 min ⁻¹ (1.86 times)	Improved	Enhanced	12.7/8.2	[96]
S	Thiourea (S and CN)	Polycondensation	2.61	–0.80	1.81	H ₂ evolution	136.0 μmol h ⁻¹ / 4.5 μmol h ⁻¹ (33.2 times)	Improved	Enhanced	128.4/12.1	[120]
S	Tri-thiocyanuric acid (S and CN)	Polycondensation	2.5	–1.15	1.35	H ₂ evolution	121 μmol h ⁻¹ / 10.1 μmol h ⁻¹ (12 times)	Improved	Enhanced	72.8/12.1	[132]
O	H ₂ O ₂ (O) dicyandiamide (CN)	Hydrothermal	2.49	–0.67	1.82	H ₂ evolution	37.5 μmol h ⁻¹ / 15.2 μmol h ⁻¹ (2.5 times)	Improved	Enhanced	47/8.2	[124]
O	H ₂ O ₂ (O) Melamine (CN)	Calcination	2.61	–	–	H ₂ evolution	60.2 μmol h ⁻¹ / 9.8 μmol h ⁻¹ (6.1 times)	Improved	Enhanced	36.1/8.2	[100]

Table 2 (Continued)

Doping element	Precursor	Synthesis	E_g (eV)	E_{CB} (eV)	E_{VB} (eV)	Application	Enhanced activity/ pristine	Light absorption	Charge separation	Modified surface area/ pristine, $m^2 g^{-1}$	Reference
O	$HNO_3 + H_2SO_4$ (O) Melamine (CN)	Chemical oxidation	2.95	−1.16	1.79	H_2 evolution	189.3 $\mu\text{mol h}^{-1}$ / 36.3 $\mu\text{mol h}^{-1}$ (5.2 times)	Improved	Enhanced	109.3/5.38	[101]
O	H_2O_2 (O) Melamine (CN)	Photo-Fenton oxidation	2.434	−	−	H_2 evolution	202.56 $\mu\text{mol h}^{-1}$ / 70.65 $\mu\text{mol h}^{-1}$ (2.9 times)	Improved	Enhanced	348/46	[102]
C	Melamine pretreated with absolute ethanol	Polycondensation	2.65	−0.95	1.70	RhB degradation	0.0362 min^{-1} / 0.0081 min^{-1} (4.47 times)	Improved	Enhanced	34/8	[60]
C	Melamine and melamine porous resin foam	Polycondensation	2.05	−0.82	1.23	NO removal	0.95 min^{-1} / 0.25 min^{-1} (3.8 times)	Improved	Enhanced	65/11	[98]
C	Glucose (C) Melamine (CN)	Hydrothermal	2.0	−	−	4-nitrophenol degradation	Enhanced	Improved	Enhanced	Increased	[128]
N	Hydrazine hydrate (N) Melamine (CN)	Polycondensation	2.65	−0.98	1.67	Hydrogen evolution	44.28 $\mu\text{mol h}^{-1}$ / 7.86 $\mu\text{mol h}^{-1}$ (5.6 times)	Improved	Enhanced	9.78/9.21	[99]
B	Boron oxide (B) Melamine (CN)	Co-polycondensation	2.66	−	−	RhB degradation	0.199 min^{-1} / 0.055 min^{-1} (3.6 times)	Improved	Enhanced	30/10	[129]
B	Ph_4BNa (B) Urea (CN)	Co-polycondensation	2.83	−	−	H_2 evolution	278 $\mu\text{mol h}^{-1}$ / 111 $\mu\text{mol h}^{-1}$ (2.50 times)	Improved	Enhanced	144/80	[130]
B	H_3BO_3 (B) Thiourea (CN)	Co-polycondensation	2.42	−1.23	1.19	UO_2^{2+} reduction	0.13 min^{-1} / 0.052 min^{-1} (2.54 times)	Improved	Enhanced	5.5/5.7	[103]
F	NH_4F (F) Dicyanamide (CN)	Co-polycondensation	2.63	−	−	H_2 evolution	2.7 times	Improved	−	38/8	[106]
I	ammonium iodine (I) Dicyanamide (CN)	Co-condensation	2.69	−	−	H_2 evolution	38 $\mu\text{mol h}^{-1}$ / 14 $\mu\text{mol h}^{-1}$ (2.7 times)	Improved	Enhanced	23/12	[104]
I	Iodine (I) Melamine (CN)	Ball milling	2.37	−1.32	1.05	H_2 evolution	44.5 $\mu\text{mol h}^{-1}$ / 4.9 $\mu\text{mol h}^{-1}$ (9.1 times)	Improved	Enhanced	80.2/10	[61]
Br	ammonia bromine (Br) Urea (CN)	Co-condensation	2.82	−	−	H_2 evolution	48 $\mu\text{mol h}^{-1}$ / 20 $\mu\text{mol h}^{-1}$ (2.4 times)	Improved	Enhanced	54/53	[105]

significantly influence the photocatalytic properties of prepared catalysts [36,109]. Therefore, many other phosphorus sources have been applied for designing P doped g-C₃N₄, such as diammonium hydrogen phosphate [109], 2-aminoethylphosphonic acid [92,110], (hydroxyethylidene) diphosphonic acid [111], hexachlorocyclotriphosphazene [9,50], ammonium hexafluorophosphate [112], phosphorous acid [93], etc. Zhou et al. synthesized P-doped g-C₃N₄ using hexachlorocyclotriphosphazene (HCCP) as phosphorus source and guanidiniumhydrochloride as g-C₃N₄ precursor by a thermally polymerization route [50]. Inspired by the compound HCCP composing of an s-triazine-like P–N heterocyclic ring, it can match well with the tri-s-triazine C–N aromatic ring structure of g-C₃N₄, and thus will highly favour the incorporation of the P atom into the framework of g-C₃N₄. Moreover, the P atoms were found to be favorably situated at the corner carbon and bay-carbon sites. As a consequence, the P atoms were easily incorporated into the g-C₃N₄ lattice, altering the electronic properties of g-C₃N₄ and suppressing the recombination of charge carriers, leading to excellent photocatalytic performance both in H₂ generation and the degradation of RhB. In another study, Hu et al. prepared phosphorus-doped g-C₃N₄ by utilizing dicyandiamide as the g-C₃N₄ precursor and diammonium hydrogen phosphate (NH₄)₂HPO₄ as the phosphorus source [109]. The introduction of phosphorus could inhibit the crystal growth of g-C₃N₄, narrow the band gap and increase the separation efficiency of photogenerated electrons and holes. However, phosphorus atoms were interstitially doped into the g-C₃N₄ lattice to generate the P–N bonds, in contrast to the work reported by Zhou et al. which suggested that P atoms was preferentially situated in the substitutional corner carbon and bay-carbon sites. Therefore, this clearly infers that the phosphorus precursor can strongly influence the P doping site either interstitial or substitutional doping.

Generally, nanostructures with specific morphologies can not only contribute to facilitate the separation and movement of photogenerated electrons and holes pairs at the materials interface but also accelerate mass transfer and supply sufficient active sites for photocatalytic reaction [111]. Nowadays, many diverse types of g-C₃N₄ nanostructures including nanosheet, nanotubes, mesostructures, nanorods, and nanofibers with enhanced performance have been designed. The combination of substitutional P doping and structural engineering has been used to design efficient g-C₃N₄ photocatalyst. For instance, Zhu et al. synthesized phosphorus-doped g-C₃N₄ nanostructured flowers of in-plane mesopores by a co-condensation of melamine and (hydroxyethylidene)diphosphonic acid [111]. They found that the P species can chemically bond with the C and N neighbors and force planar coordination in the carbon nitride framework. Moreover, the lone electron pair can delocalize to the π -conjugated tri-s-triazine of P-doped g-C₃N₄ that can enhance the conductivity and electron transfer capability by serving as reinforcing active sites to some extent [113]. The reduced thickness and the well-developed in-plane mesopores can shorten charge transfer length from the bulk to the interface [114], where the photoredox reaction takes places. Therefore, the resulting flower-like morphology together with the doping of phosphorus markedly increased the specific surface area due to high porosity, improved mass transfer of reactant and product molecules, excellent trapping of light and importantly, superior charge transfer and separation for excellent hydrogen evolution under visible light.

In addition to mesoporous P-doped g-C₃N₄ nanoflowers, porous P-doped g-C₃N₄ nanosheets by a combination of P doping and thermal exfoliation using 2-aminoethylphosphonic acid (AEP) as the novel phosphorus source were developed by Qiao's group for insightful understanding of the effect of P doping on the band gap structure and photocatalytic performance [92]. XPS results suggested that P most probably substituted C in g-C₃N₄ to form P–N bonds. Moreover, the DFT calculation results further indicated that

the more energy-favorable C site for P doping was C1 instead of C2 in the heptazine unit (Fig. 4a). As shown in Fig. 4b–c, the further observation on the (100) and (002) peaks of P-doped g-C₃N₄ and pure g-C₃N₄ confirmed the calculation results. Even though the previous reported studies highlight the advantages of exfoliated g-C₃N₄ from the bulk counterpart, the main bottleneck of the thermally exfoliated g-C₃N₄ nanosheets is the enlarged band gap energy, which greatly suffers from the utilization of wide spectrum of solar light [53,115,116]. In this study, the thermal exfoliation enlarges the band gap of PCN-S to 2.91 eV, due to the strong quantum confinement effect (QCE) aroused by the ultrathin nanosheet structure [53,116]. However, the band gap of P-doped g-C₃N₄ can be reduced with the presence of strong tail absorption (Urbach tail), which was responsible for the formation of midgap states within the band gap [117]. In fact, the intrinsic band gap of g-C₃N₄ was drastically decreased from 2.98 to 2.66 eV after P doping supported by the DFT studies (Fig. 4d–e). As depicted in Fig. 5f, the midgap states induced by P doping can extend the visible-light absorption region from 429 nm up to 557 nm. In another study, Deng et al. prepared P doped porous ultrathin g-C₃N₄ nanosheets by the above method with some modifications and applied for highly efficient simultaneous photocatalytic removal of Cr (VI) and 2,4-dichlorophenol [110]. Additionally, Guo et al. developed P doped hexagonal tubular g-C₃N₄ (P-TCN) with the layered stacking structure. The synthesis routes of P-TCN involves two steps (Fig. 5a): 1) under phosphorous acid-assisted hydrothermal conditions, the supramolecular precursor was obtained by self-assembly of melamine and cyanuric acid; 2) P from phosphorous acid squeezed into the g-C₃N₄ skeleton under heating, thus giving the hexagonal P-TCN (Fig. 5b–e). The tubular structure promotes favors the enhancement of light scattering (Fig. 5f) and active sites. Meanwhile, phosphorus doping leads to an arrow band gap (Fig. 5f) and increased electric conductivity. Therefore, the P-TCN displayed a high hydrogen evolution rate of 670 $\mu\text{mol h}^{-1} \text{g}^{-1}$ (Fig. 5h), and an apparent quantum efficiency of 5.68% at 420 nm.

3.2. Sulfur doping

Sulfur doping has also been used to modify the electronic structure of g-C₃N₄ for enhanced light absorbance, redox potential, charge-carrier mobility, and consequently, photoreactivity [94–97,118–120]. Liu et al. first prepared sulfur-doped g-C₃N₄ by treating pure g-C₃N₄ powder in gaseous H₂S atmosphere at 450 °C [94]. The S-doped g-C₃N₄ displays an increased VB width in combination with an elevated CB minimum and a slightly reduced absorbance. This unique electronic structure, which caused by the homogeneous substitution of sulfur for lattice nitrogen and a concomitant quantum confinement effect, leads to S-doped g-C₃N₄ with excellent photoreduction of H₂ evolution and photooxidation of phenol. In another study, nanoporous sulfur-doped g-C₃N₄ microrods were prepared by direct thermal condensation of melamine and trithiocyanuric acid supramolecular cocrystal under N₂ atmosphere [121]. The obtained S-doped g-C₃N₄ with larger surface area and enhanced visible light absorption afforded an activity about 9.3 times higher than that of pure g-C₃N₄ for H₂ evolution and exhibited satisfactory stability. Recently, Fan et al. prepared S-doped g-C₃N₄ porous rods using the same precursors with enhanced photocatalytic activity for RhB degradation under visible light [119]. The synergistic effects of sulfur doping and the particular structure made S-doped g-C₃N₄ with larger surface areas, broader light adsorption range and narrower band gaps than that of bulk g-C₃N₄, resulting in improved photocatalytic activity.

As described above, both ex situ and in situ sulfur doping with small percentages of sulfur (<1.0 wt%) have been revealed to be an effective way to improve the photocatalytic performances of g-C₃N₄. Recently, thiourea (TU) has also been reported to be an effi-

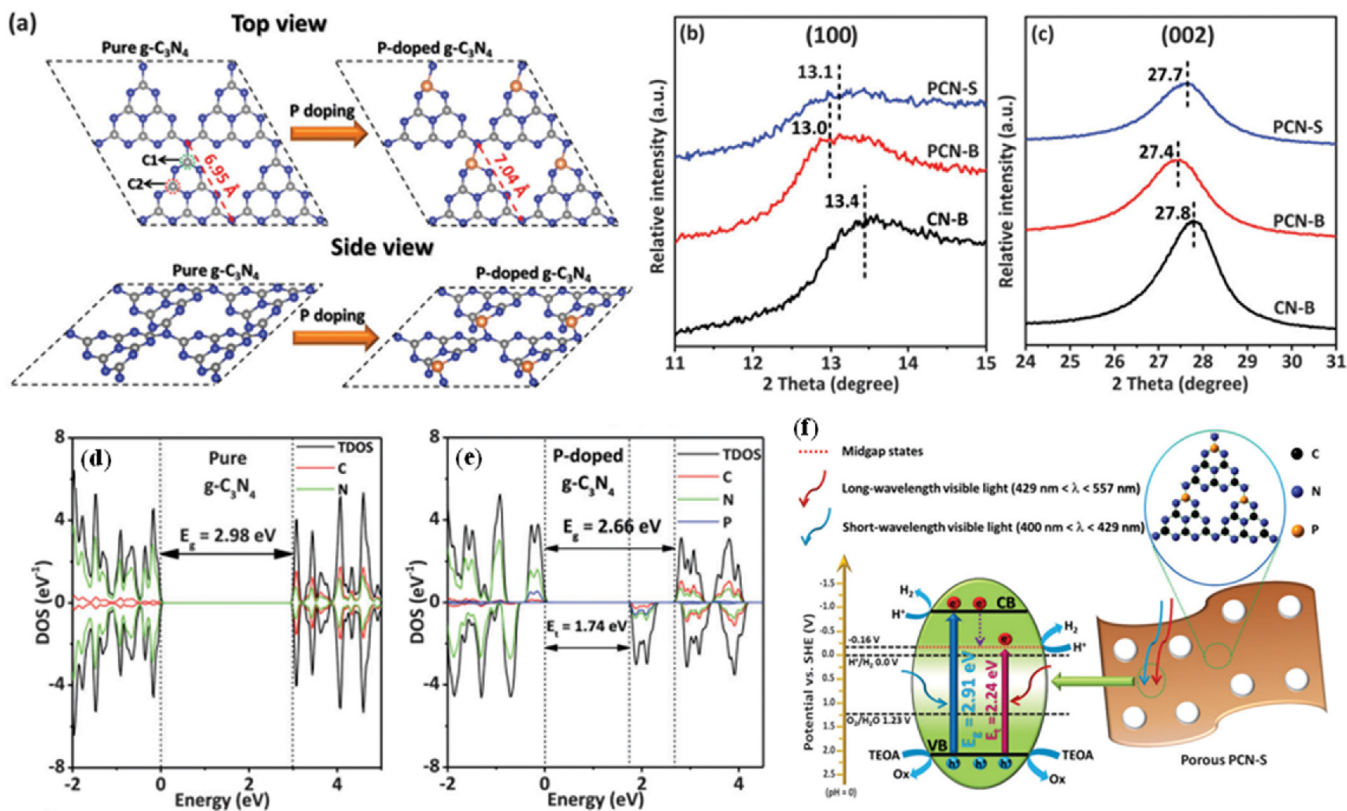


Fig. 4. (a) Top and side view of the optimized pure g-C₃N₄ and P-doped g-C₃N₄ configuration, color scheme: C, grey; N, blue; P, orange. Enlarged view of (100) peaks (b) and (002) peaks (c) for CN-B, PCN-B and PCN-S. Total density of states (TDOS) and partial density of states (PDOS) of (d) the pure g-C₃N₄ and (e) the P-doped g-C₃N₄. The Fermi level is set to the zero of energy. Photocatalytic H₂-production mechanism of porous PCN-S. Reprinted with permission from ref. [92] Copyright 2015 Royal Society of Chemistry.

cient precursor for both g-C₃N₄ and in situ S doping to construct S-doped g-C₃N₄ [95,96,120,122]. Hong et al. first synthesized in situ S doped mesoporous g-C₃N₄ (mpgCNS) from single thiourea [120]. XPS analysis result indicated that the doped sulfur would substitute carbon in mpgCNS and a downshift of 0.25 eV was found in its CB. The obtained mpgCNS exhibited 30 times more active than the pure g-C₃N₄ for H₂ evolution with a high quantum efficiency of 5.8% at 440 nm. The enhanced photocatalytic activity was attributed to the effect of stronger and extended light absorbance by sulfur doping and more efficient mass and charge transfer in the mesoporous structure. However, other published papers reported that S doping was proposed to substitute the lattice N atoms rather than C atoms in the g-C₃N₄ to yield a S–C bond [95,96]. In view of the similar electro-negativities of sulfur and nitrogen, the replacement of the edge of the N atom of g-C₃N₄ with the S atom was practically favorable, which was consistent with the DFT studies investigated by Ma et al. [123]. Wang et al. further fabricated sulfur-doped g-C₃N₄ by simply calcinating thiourea and applied for CO₂ reduction by photocatalysis to CH₃OH with a yield of 1.12 μmol g⁻¹, compared to 0.81 μmol g⁻¹ on the undoped sample [95]. The unit cells of pure g-C₃N₄ (MCN) and S-doped C₃N₄ (TCN) used in the first-principle calculations are shown in Fig. 6a–b. For the simulation of S-doped g-C₃N₄, one S atom was introduced by substituting one bidentate N atom in the supercell (Fig. 6b). The TEM images in Fig. 6c showed TCN were grainy in structure, and their layered structures contain many irregular pore sizes. In Fig. 6d, the S 2p peak at 164 eV was ascribed to C–S bond formed by substituting lattice nitrogen with sulfur. As depicted in Fig. 6e, S-doped g-C₃N₄ can enlarge light absorption up to 475 nm and narrow the band gap to 2.63 eV. Photoluminescence and photocurrent mea-

surements illustrated that TCN has higher separation efficiency of electron–hole pairs. Furthermore, first-principles studies showed that the band gap was not changed by the doping, however impurity states appeared. Thus, photogenerated electrons could easily jump from the VB to the impurity state or from the impurity state to the CB. The photocatalytic reduction of soluble U(VI) to insoluble U(IV) oxide was conducted by S-doped g-C₃N₄ with high efficiency which is 1.86 and 32 times of that for pristine g-C₃N₄ and N-TiO₂ under visible light irradiation [96]. Both experimentally and theoretically study identified that doping sulfur for substituting the lattice nitrogen modified the electronic structure of g-C₃N₄, resulting in a narrowed band-gap with the tuned CB and VB levels alone with efficient electron–hole separation and carrier mobility.

3.3. Oxygen doping

Oxygen-doped g-C₃N₄ was synthesized for the first time by Li et al. using a facile H₂O₂ hydrothermal approach [124]. XPS results showed that oxygen was doped into the lattice and then formed N–C–O, which indicated that O atoms could be directly bonded to sp²-hybridized carbon. Importantly, a downshift of the CB minimum by 0.21 eV was confirmed by the oxygen doping without modifying the VB maximum. Thus, the O-doping in the g-C₃N₄ lattice could induce intrinsic electronic and band structure modulation, leading to improved surface area, extended visible light response, and enhanced separation efficiency of the photo-generated charge carriers. In another study, Huang et al. treated melamine with H₂O₂ to form hydrogen bond induced supramolecular aggregates (denoted as MHP), and then synthesized g-C₃N₄ with simultaneous porous network and O-doping (denoted as

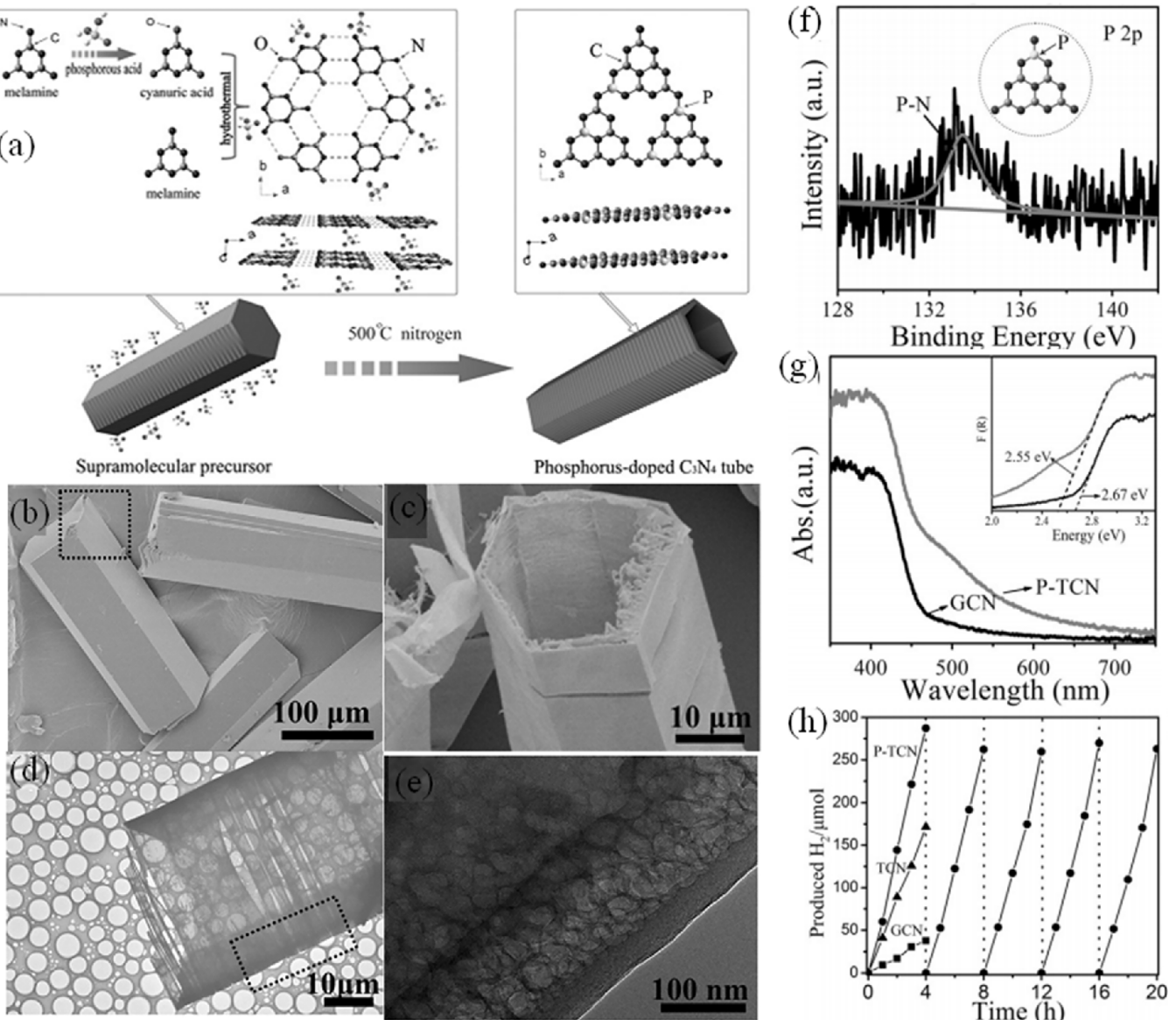


Fig. 5. (a) The formation process of phosphorus-doped tubular carbon nitride. SEM images of supramolecular precursor (b) and P-TCN (c). (d-e) TEM images of P-TCN. (f) high-resolution XPS spectra of P-TCN: P 2p. (g) UV/Vis light absorption spectra and band gap energies (inset) of GCN and P-TCN. (f) Time course of H_2 evolution for GCN, TCN, and P-TCN under visible light irradiation. Reprinted with permission from ref. [93] Copyright 2016 John Wiley & Sons, Inc.

MCN) by condensation of MHP (Fig. 7a) [100]. XPS spectra displayed a new peak at low binding energy of 531.4 eV appears for MCN, which can be attributed to the C–O and N–C–O species in lattice. According to DFT calculation, the band gap becomes narrowed slightly after O doping (Fig. 7b), which is in agreement with the red shift of absorption band edge. In addition, the differential charge density results indicated that the electron density is dramatically reduced at the neighboring C atoms of O dopant, along with significant increase at the neighboring N atoms (Fig. 7c). Therefore, based on experimental and DFT computation, they concluded that O doping preferentially occurs on two-coordinated N position (Fig. 7d), and the porous network and O-doping synergistically promote the light harvesting and charge separation. As a result, MCN-1 shows much enhanced photocatalytic activity for pollutant degradation (Fig. 7e) and hydrogen evolution (Fig. 7f). It is known that 2D $\text{g-C}_3\text{N}_4$ is beneficial to interface photoexcited charge transfer and can possess the quantum confinement effect [125,126]. Thus, She et al. prepared 2D porous ultra-thin O-doped $\text{g-C}_3\text{N}_4$ nanosheets by a facile strategy to modulated the morphology, intrinsic electronic

structure and band positions of the bulk $\text{g-C}_3\text{N}_4$ simultaneously [101]. Ultra-thin $\text{g-C}_3\text{N}_4$ nanosheets was first prepared by the calcined method, and then the mixed acid (H_2SO_4 and HNO_3) was applied for chemical oxidation of $\text{g-C}_3\text{N}_4$ nanosheets to obtain porous ultra-thin O-doped $\text{g-C}_3\text{N}_4$ nanosheets. The photocatalytic activity of ultra-thin O-doped $\text{g-C}_3\text{N}_4$ nanosheets for H_2 evolution and MO degradation is almost 5.2 times and 71 times higher than that of the bulk $\text{g-C}_3\text{N}_4$. The improved photocatalytic activity is ascribed to the synergistic effects of 2D porous ultrathin structure, the introduction of the electrophilic groups (C–O, C=O and COOH) and the increased bandgap. In another paper, a holey structured $\text{g-C}_3\text{N}_4$ nanosheet with edge oxygen doping was successfully designed by using photo-Fenton reaction [102]. The as-prepared O-doped holey structured $\text{g-C}_3\text{N}_4$ nanosheet demonstrated a narrow bandgap of 2.434 eV and high surface area of $348 \text{ m}^2 \text{ g}^{-1}$, thus leading to highly efficient photocatalytic activity for H_2 generation and RhB degradation under solar light irradiation.

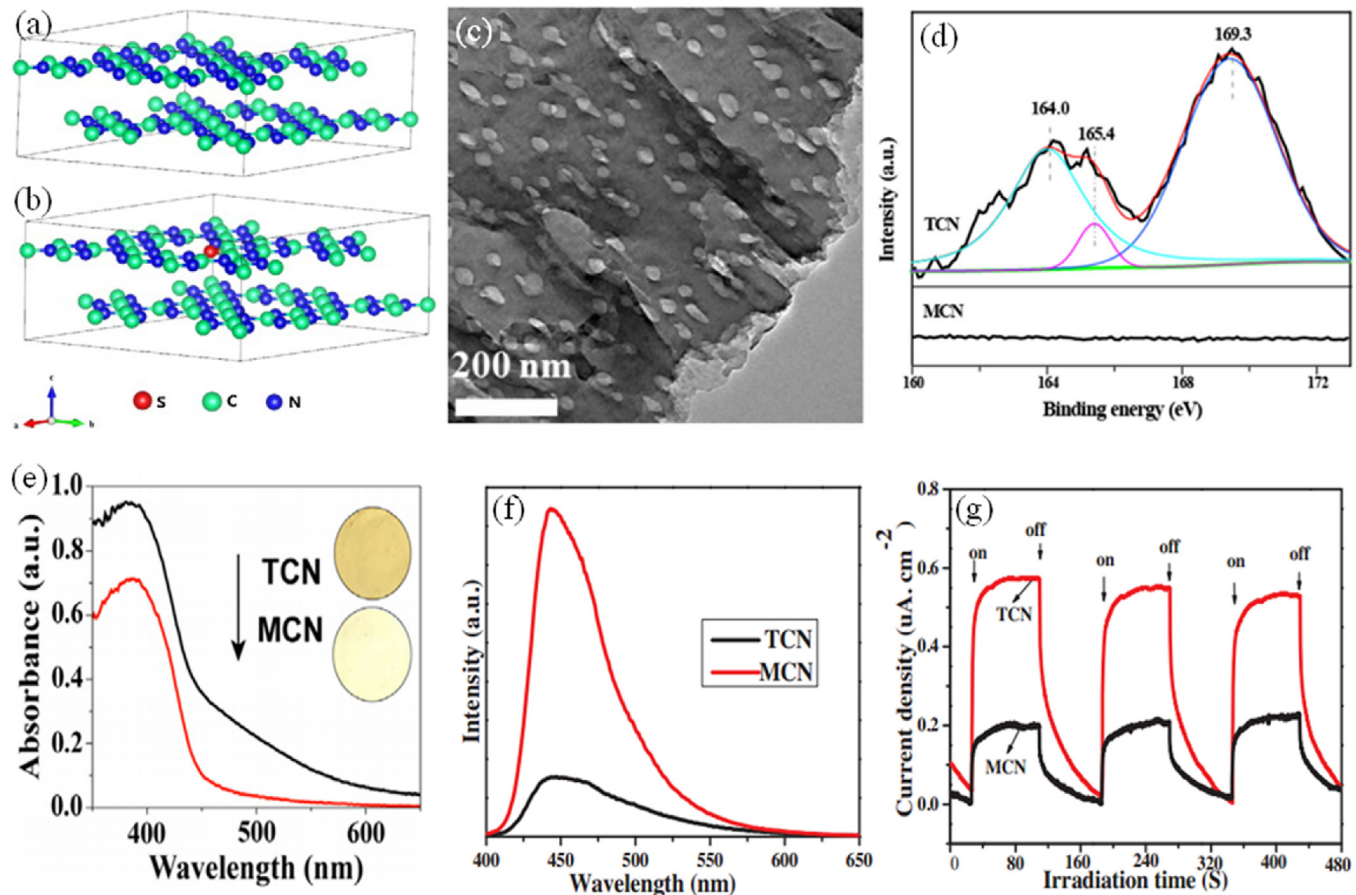


Fig. 6. (a) Supercell of pure g-C₃N₄. (b) Supercell of S-doped g-C₃N₄. (c) TEM images of TCN (S-doped g-C₃N₄). (d) high-resolution XPS spectra of S2p for TCN. (e) UV-vis diffuse reflection spectra and corresponding colors (inset) of TCN and MCN (pure g-C₃N₄). (f) Photoluminescence (PL) spectra of TCN and MCN. (g) Transient photocurrent responses of TCN and MCN. Reprinted with permission from ref. [95] Copyright 2015 Elsevier.

3.4. Carbon, nitrogen or boron doping

Through the first-principles DFT calculations, Dong et al. found that the substitution of bridging N atoms with C atoms in g-C₃N₄ would lead to the formation of delocalized big π bonds among the substituted carbons and the hexatomic rings, which would boost electrical conductivity of g-C₃N₄ [60]. Additional, the carbon self-doping would also narrow the band gap of g-C₃N₄, which thus enhance the visible light absorption. Thus, they synthesize carbon self-doped g-C₃N₄ by using melamine pretreated with absolute ethanol as the precursor to provide more carbon. Consistent with the theoretical calculation results, the obtained carbon self-doped g-C₃N₄ displayed enhanced visible light absorption and electrical conductivity as well as surface area and thus improved photocatalytic performance. A similar observation was also analyzed by Zhao et al., who developed carbon self-doped g-C₃N₄ photocatalysts by employing the polyporous carbon foam as a soft template for high photocatalytic activity toward purification of NO in air [98]. Furthermore, they found that C-doped g-C₃N₄ displayed high BET surface area (65 m² g⁻¹), extended absorption up to near-infrared range (800 nm) and accelerated electrons-holes separation. In another study, Li et al. prepared C-doped g-C₃N₄ by facilely hydrothermal treatment of the mixture of g-C₃N₄ and glucose solution for enhanced MB photodegradation [127]. Afterward, Zhang et al. developed a hydrothermal synthesis of the novel C-doped g-C₃N₄ (CCN) nanosheet by using melamine and glucose as the precursors [128]. Importantly, due to the introduction of car-

bon doped in CN framework, two advantages are found in CCN: (a) Improved electrical conductivity because delocalized big π bonds among the carbons favor the electrons transfer; (b) Enhanced light absorption wavelength because of the narrower band gap.

Nitrogen self-doped g-C₃N₄ (C₃N_{4+x}) was successfully synthesized by thermal condensation of melamine pretreated with hydrazine hydrate to provide more nitrogen [99]. XPS indicated the sp² carbon atom was substituted by the nitrogen atom with five outer shell electrons (Fig. 8a). The UV-vis spectra showed N-doping could weak red-shift of the light adsorption band edge of g-C₃N₄ and decrease band gap from 2.72 eV (g-C₃N₄) to 2.65 eV (Fig. 8b). Fig. 8c indicated that the valence band maximum of g-C₃N₄ and C₃N_{4+x} was at 1.84 eV and 1.76 eV, respectively. The EPR results proved that the electronic structure of g-C₃N₄ after nitrogen self-doping had been modified (Fig. 8d). Meanwhile, N doping greatly promoted the charge separation and mobility efficiency, of the charge carriers (Fig. 8e–f). As a result, N-doped g-C₃N₄ showed superiority in photocatalytic hydrogen evolution than pure g-C₃N₄ under visible light irradiation.

Boron-doped g-C₃N₄ were first reported by Yan et al. via heating the mixture of melamine and boron oxide [129]. Typically, the mixed precursors were heated to 500 °C in a muffle furnace for 2 h and further heat treated at higher temperature for 2 h. In the first stage, the pyrolysis of melamine would take place to form g-C₃N₄ with residual C–NH₂ and 2C–NH. However, the B₂O₃ did not react with melamine at temperatures lower than 520 °C under ambient temperature. Therefore, further increasing the heat treat-

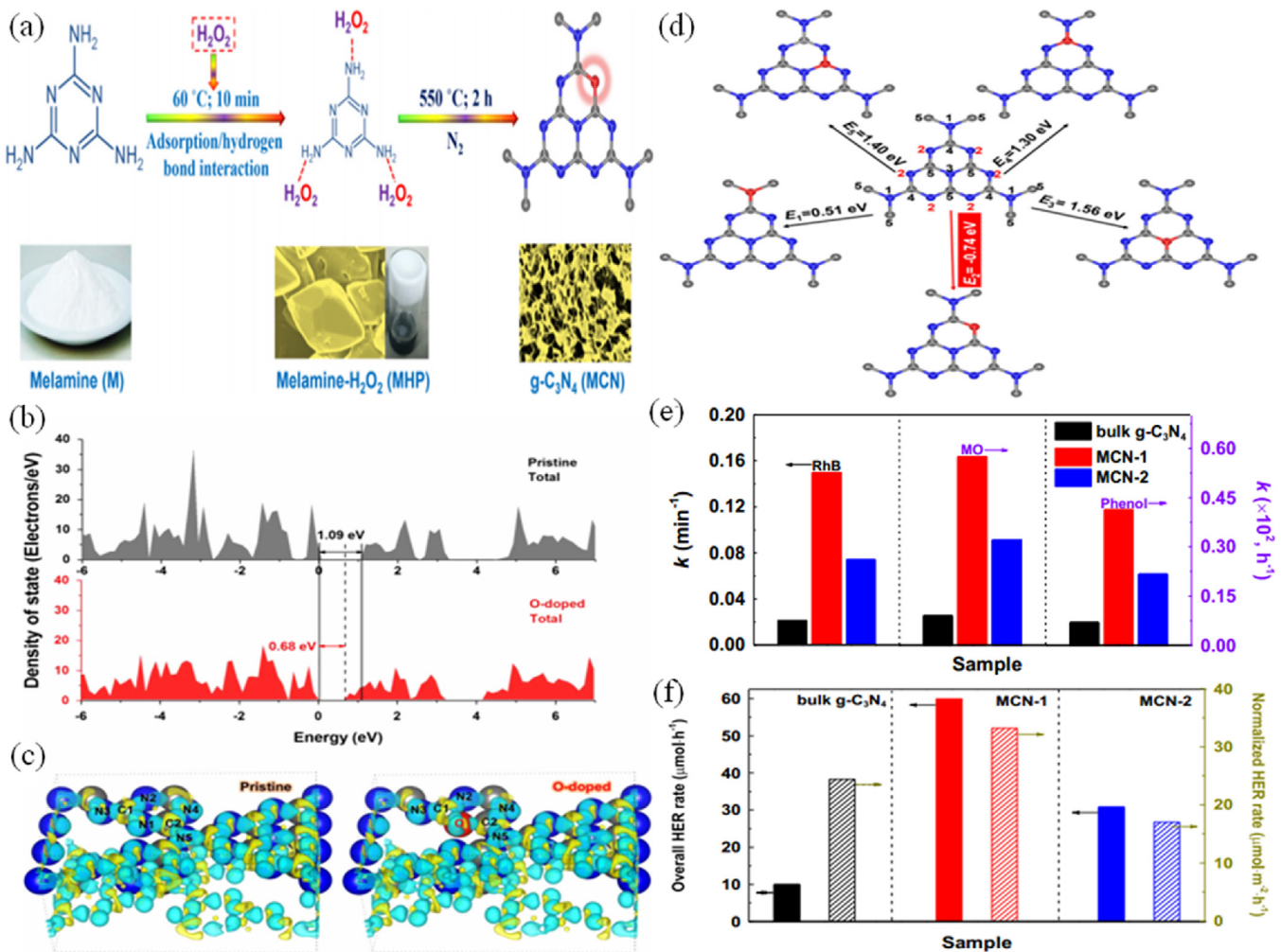


Fig. 7. (a) Fabrication of O-doped g-C₃N₄ (C, N and substitutional O are indicated by gray, blue and red spheres, respectively). (b) calculated DOS plots and (c) differential charge density of pristine and O-doped g-C₃N₄. The differential charge density illustrates the increase (cyan color) and decrease (olive color) of electron distributions. (d) Calculated formation energy of O-doped g-C₃N₄ by substituting N (site 1–3) and C (site 4, 5) atoms using O atom. (e) photodegradation reaction rates of RhB, phenol and MO. (f) HER rate of powder catalysts. Reprinted with permission from ref. [100] Copyright 2015 Elsevier. (For interpretation of the references to colour in this figure legend, the reader is referred to the web version of this article.)

ment temperature above 520 °C, the C–NH₂ and 2C–NH react with B₂O₃, and 2C–NB and C–NB₂ groups were formed. As expected, B doping could slightly narrow the band gap of g-C₃N₄ from 2.75 to 2.66 eV along with improved optical absorption, which promote photodegradation of RhB. In another study, Lin and Wang synthesized B-doped g-C₃N₄ samples by one-pot thermal polymerization of urea and Ph₄BNa for photocatalytic water splitting [130]. They found that Ph₄BNa was served as a dual-function modifier for the polycondensation of urea as it contained phenyl leaving groups and B atoms doping. The specific surface area can be enlarged by B doping and the electronic structure of CN can be altered by creating polar surface docking sites. Moreover, the additional boron functional groups on the surface might act as Lewis acid sites. Therefore, the B-doped g-C₃N₄ show much higher hydrogen evolution activity. Besides that, B doped g-C₃N₄ has been prepared by other precursors for efficient B doping. For example, Sagara et al. prepared a p-type B-doped g-C₃N₄ electrode using BH₃NH₃ as the dopant precursor, which demonstrated improved CO₂ reduction [62]. Lu et al. constructed efficient B-doped g-C₃N₄ photocatalysts by co-polycondensation of thiourea and H₃BO₃ for the photocatalytic reduction of UO₂²⁺ [103]. They found that narrowed band gap and enhanced absorption intensity of visible-light was obtained

after B doping, and leading to the improved photocatalytic activity for UO₂²⁺ removal.

3.5. Halogen doping

Fluorine-doped g-C₃N₄ was obtained by incorporating NH₄F into the g-C₃N₄ framework [106]. Due to the electronegativity of nitrogen and fluorine, the doped fluorine would bind easily to the carbon instead of nitrogen, resulting in the partial conversion of C-sp² to C-sp³. Hence, the doping of fluorine formed the C–F bonding, which in turn decrease in band gap from 2.69 eV of g-C₃N₄ to 2.63 eV. Moreover, DFT calculations indicated that the incorporation of F at the bay carbon shifts both the VB and CB to higher energy values. In photocatalytic hydrogen evolution, F doped g-C₃N₄ demonstrated about 2.7 times higher activity than the unmodified g-C₃N₄. Besides this, iodine-modified g-C₃N₄ was synthesized by the co-condensation of dicyandiamide and ammonium iodine [104]. The experiment results showed that I doping endows g-C₃N₄ with enlarged surface area, improved optical absorption, and accelerated charge carriers separation rate as well as the increased hydrogen evolution rate. DFT calculations indicated that the sp²-bonded N is prone to be substituted by I atom. The interaction between iodine and carbon nitride extended the π -conjugated sys-

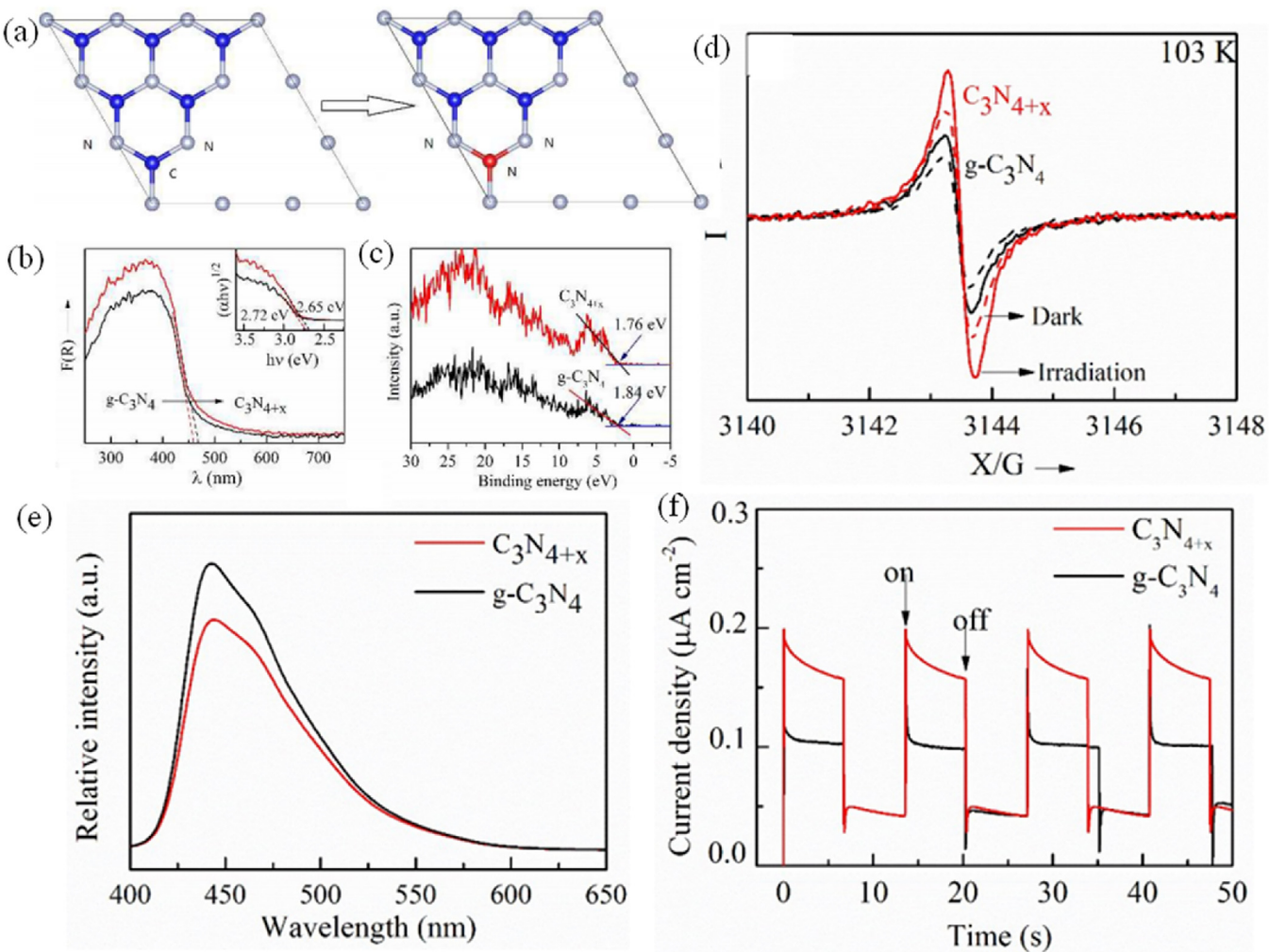


Fig. 8. (a) Schematic structure transformation for $\text{g-C}_3\text{N}_4$ before and after nitrogen self-doping; red: substituting nitrogen atom, blue: nitrogen atom, gray: carbon atom. (b) UV–vis diffuse reflectance spectra and (c) high-resolution valence band XPS spectra of C_3N_{4+x} and $\text{g-C}_3\text{N}_4$. (d) EPR spectra of C_3N_{4+x} and $\text{g-C}_3\text{N}_4$ in the dark and after visible light irradiation. (e) photoluminescence spectra and (f) transient photocurrent response of C_3N_{4+x} and $\text{g-C}_3\text{N}_4$. Reprinted with permission from ref. [99] Copyright 2015 Royal Society of Chemistry.

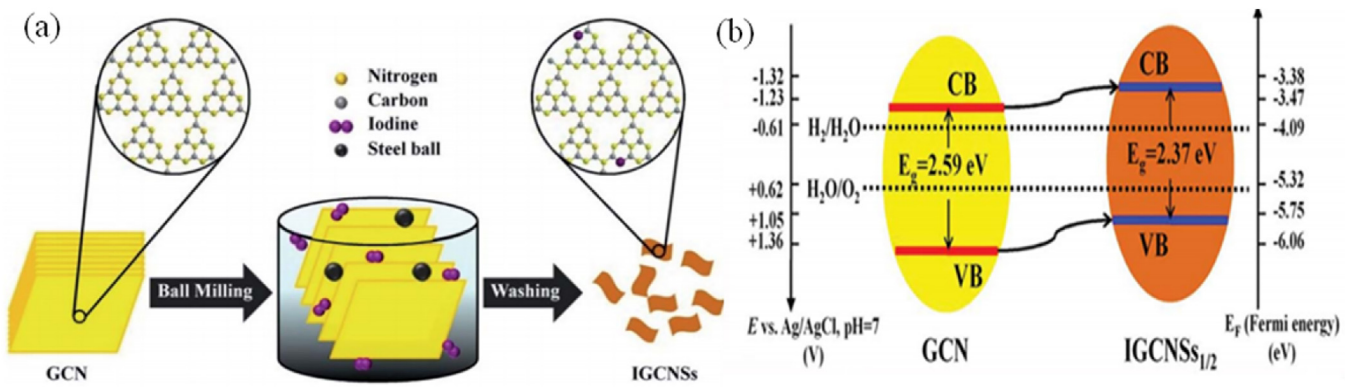


Fig. 9. (a) Schematic of ball-milling process for I-doped $\text{g-C}_3\text{N}_4$. Yellow, gray, purple and black spheres stand for nitrogen atoms, carbon atoms, iodine atoms and steel balls, respectively. (b) Schematic illustration of electronic structures of $\text{IGCNSs}_{1/2}$ compared to that of the bulk GCN. Reprinted with permission from ref. [61] Copyright 2015 Royal Society of Chemistry. (For interpretation of the references to colour in this figure legend, the reader is referred to the web version of this article.)

tem might be beneficial to the transfer of photogenerated carriers. In another study, I doped $\text{g-C}_3\text{N}_4$ nanosheets was prepared by simply ball-milling bulk $\text{g-C}_3\text{N}_4$ with iodine (Fig. 9a) [61]. Compared to those of the bulk GCN, both the VB maximum and the CB minimum of $\text{IGCNSs}_{1/2}$ are up shifted, suggesting that the $\text{IGCNSs}_{1/2}$

have a narrower bandgap and better aligned energy levels (Fig. 9b). Due to the enlarged specific surface area, efficient light absorption, improved charge separation, narrower bandgap and better aligned band structure, the IGCNSs samples show enhanced photocatalytic H_2 production activities under the visible-light irradiation.

Another halogen element, bromine, was also applied to prepare doped $g\text{-C}_3\text{N}_4$ by co-condensation of urea and ammonia bromine [105]. They found that the incorporation of bromine into $g\text{-C}_3\text{N}_4$ framework indeed modulated the texture, optical absorption, electron conductivity, charge-carrier separation rate. The optimal sample exhibited more than two times higher H_2 evolution rates than pure CNU sample with high stability under visible light irradiation. The photocatalytic O_2 evolution activity of CNU-Br0.1 was also enhanced. Furthermore, dicyandiamide, urea, thiourea, and ammonium thiocyanide can also modified by this method.

4. Co-doping

Codoping or tridoping could combine the advantages of these single dopants, leading to enhanced photocatalytic activity. This approach has been widely used in TiO_2 modification [29,133–135]. Recently, dual doping of $g\text{-C}_3\text{N}_4$ by codoping nonmetal or metal ions is gaining attention as this approach exhibits positive influences on the structural and optical properties. Zhao et al. prepared band-tunable K-Na co-doped $g\text{-C}_3\text{N}_4$ by molten salt method using melamine, KCl, and NaCl as precursor [136]. Through controlling the weight ratio of eutectic salts to melamine, the CB and VB potentials of $g\text{-C}_3\text{N}_4$ could be tuned from -1.09 and $+1.55$ eV to -0.29 and $+2.25$ eV. XPS results indicated that the ions of K and Na are coordinated into the big C–N rings, which means interstitial doping but not substitutional doping. The photodegradation and mineralization performances of RhB were significantly enhanced after K-Na co-doping because of enlarged surface area and increased the separation rate of photogenerated charges. In another study, metal/nonmetal doping was developed by Hu et al. via using dicyandiamide, ferric nitrate, and diammonium hydrogen phosphate as precursor to obtain Fe and P co-doped $g\text{-C}_3\text{N}_4$ [137]. It was found that the phosphorus atom was doped into $g\text{-C}_3\text{N}_4$ to form the P–N bonds at the interstitial sites of $g\text{-C}_3\text{N}_4$. Meanwhile, the Fe atom was coordinated to the N atoms at the interstitial position in the nitrogen pots of $g\text{-C}_3\text{N}_4$. The improved activity was due to the synergistic effect of Fe and P co-doping which inhibited the crystal growth of $g\text{-C}_3\text{N}_4$, enhanced the surface area, narrowed the band gap energy, and promoted the separation efficiency of photogenerated charges. Furthermore, C and Fe co-doped $g\text{-C}_3\text{N}_4$ was constructed for bandgap narrowing and obtaining a more positive valence band potential to improve visible-light-driven photocatalytic ability [138]. Experimental results show that C and Fe codoped $g\text{-C}_3\text{N}_4$ displays enhanced photocatalytic efficiency for RhB degradation compared with single-doped $g\text{-C}_3\text{N}_4$ and pristine $g\text{-C}_3\text{N}_4$ under visible-light irradiation. The synergistic enhancement could be attributed to the three features: 1) C and Fe codoping tuned the bandgap and improved visible-light absorption; 2) higher surface area and greatly enhanced photogenerated charge separation rate; and 3) both increased electrical conductivity and a more positive VB. Besides these, nonmetal/nonmetal co-doping has also been reported for enhancing the photocatalytic activity of $g\text{-C}_3\text{N}_4$. For example, Ma et al. synthesized P and O co-doped $g\text{-C}_3\text{N}_4$ for enhanced photocatalytic RhB degradation under anoxic condition, which caused by the similar effects described above, such as enlarged surface area, decreased band gap and increased separation efficiency of photo-induced charges [139]. Lin and Wang prepared B/F co-doped $g\text{-C}_3\text{N}_4$ by polymerizing urea with an ionic liquid [140]. XPS results indicated that both boron and fluorine heteroatoms have been introduced into the $g\text{-C}_3\text{N}_4$ matrix by the formation of the B–N and B–F bonds. Higher hydrogen evolution rate could be obtained due to the enhanced optical harvesting and charge separation capabilities.

Recently, tridoped $g\text{-C}_3\text{N}_4$ has also been developed by combining three different heteroatoms into $g\text{-C}_3\text{N}_4$ framework for

improved photocatalytic performances [141,142]. Ma et al. synthesize a novel S-Co–O tridoped $g\text{-C}_3\text{N}_4$ via hydrothermal post-treatment in the absence of hydrogen peroxide [141]. In this study, S and Co co-doped $g\text{-C}_3\text{N}_4$ was first prepared by annealing the mixture of thiourea and $\text{Co}(\text{NO}_3)_2\cdot6\text{H}_2\text{O}$ and then hydrothermal post-treatment to obtain S-Co–O tridoped $g\text{-C}_3\text{N}_4$. The surface area, band gap energy and the separation of the photo-induced charges have been modified. Moreover, oxygen doping not only increases the adsorption ability of $g\text{-C}_3\text{N}_4$ but also to produce photo-generated holes for RhB degradation by capturing the photogenerated electrons under anoxic conditions. Similarly, Hu et al. constructed oxygen functionalized S-P codoped $g\text{-C}_3\text{N}_4$ nanorods using an analogous annealing and hydrothermal post-treatment strategy [142]. The results indicated that P-SN(6 h) exhibits the highest RhB degradation constant (0.026 min^{-1}), which is 13 and 2 times higher than those of CN and P-SN. Generally, element doping could decreases the band gap energy and increases the separation efficiency of the photogenerated charges, thus, leading to enhanced photocatalytic activity. However, excessive doping of nonmetal and metal is found to be detrimental to the photocatalysis due to the formation of more defects for the recombination of electron–hole pairs [60,143,144].

5. Heterojunction based on doped $g\text{-C}_3\text{N}_4$

Generally, element doping is adopted as an effective strategy to improve the performance by modifying their electronic structure and surface properties of $g\text{-C}_3\text{N}_4$ for efficient photocatalyst [50,63,96,111]. The heterojunction construction is always be used to improve separation of photogenerated electrons and inhibit the electron–hole pair recombination [11,13,145]. It is expected that it is much meaningful to combine simultaneous doping and heterojunction engineering to modify $g\text{-C}_3\text{N}_4$ with a great possibility for efficient visible-light photocatalysis. Recently, many studies have focus on the development of heterojunction based on doped $g\text{-C}_3\text{N}_4$ [146–151].

The coupling of wide-band-gap inorganic semiconductor oxides with doped $g\text{-C}_3\text{N}_4$ would be beneficial on the basis of their energy band levels so as to promote the separation of photoexcited electron–hole charges. TiO_2 is the mostly popular photocatalyst because of its high chemical stability, low cost, and proper VB and CB positions for redox reactions, but restricted by its wide band gap that absorbs only a small part of the solar spectrum (UV light) [29,152–154]. Bu and Chen fabricated oxygen-doped $\text{C}_3\text{N}_4@\text{TiO}_2$ ($\text{O-C}_3\text{N}_4@\text{TiO}_2$) composites with quasi-shell-core nanostructure [155]. The results reveal that the interfacial chemical bonds formed between $\text{O-C}_3\text{N}_4$ and TiO_2 can become effective transfer channel for the photogenerated electrons and effectively reduce the recombination efficiency of the photogenerated electrons and holes. In another work, Raziq et al. synthesized boron-doped $g\text{-C}_3\text{N}_4$ nanosheets and its nanocomposites with nanocrystalline anatase TiO_2 (T/B-CN) [148]. The as-prepared T/B-CN nanocomposites exhibited rather higher cocatalyst-free photoactivities for producing H_2 and CH_4 under visible-light irradiation, compared to those of bare $g\text{-C}_3\text{N}_4$. This is attributed to the greatly enhanced photogenerated charge separation after doping boron and subsequent coupling with TiO_2 , in which B-induced surface states near the valence band top to trap holes and the formed heterojunctions to transfer electrons from B-CN to TiO_2 . In the field of photocatalysis, Al_2O_3 is also widely used as catalyst's support due to its excellent chemical stability, high specific surface area, good thermal stability and its broad band gap. Wang et al. combined $\gamma\text{-Al}_2\text{O}_3$ and hydrogen peroxidetreated $g\text{-C}_3\text{N}_4$ ($\text{O-g-C}_3\text{N}_4$) via a novel in-situ hydrothermal method [156]. They found that the photocatalytic activity improvement for water splitting was caused by

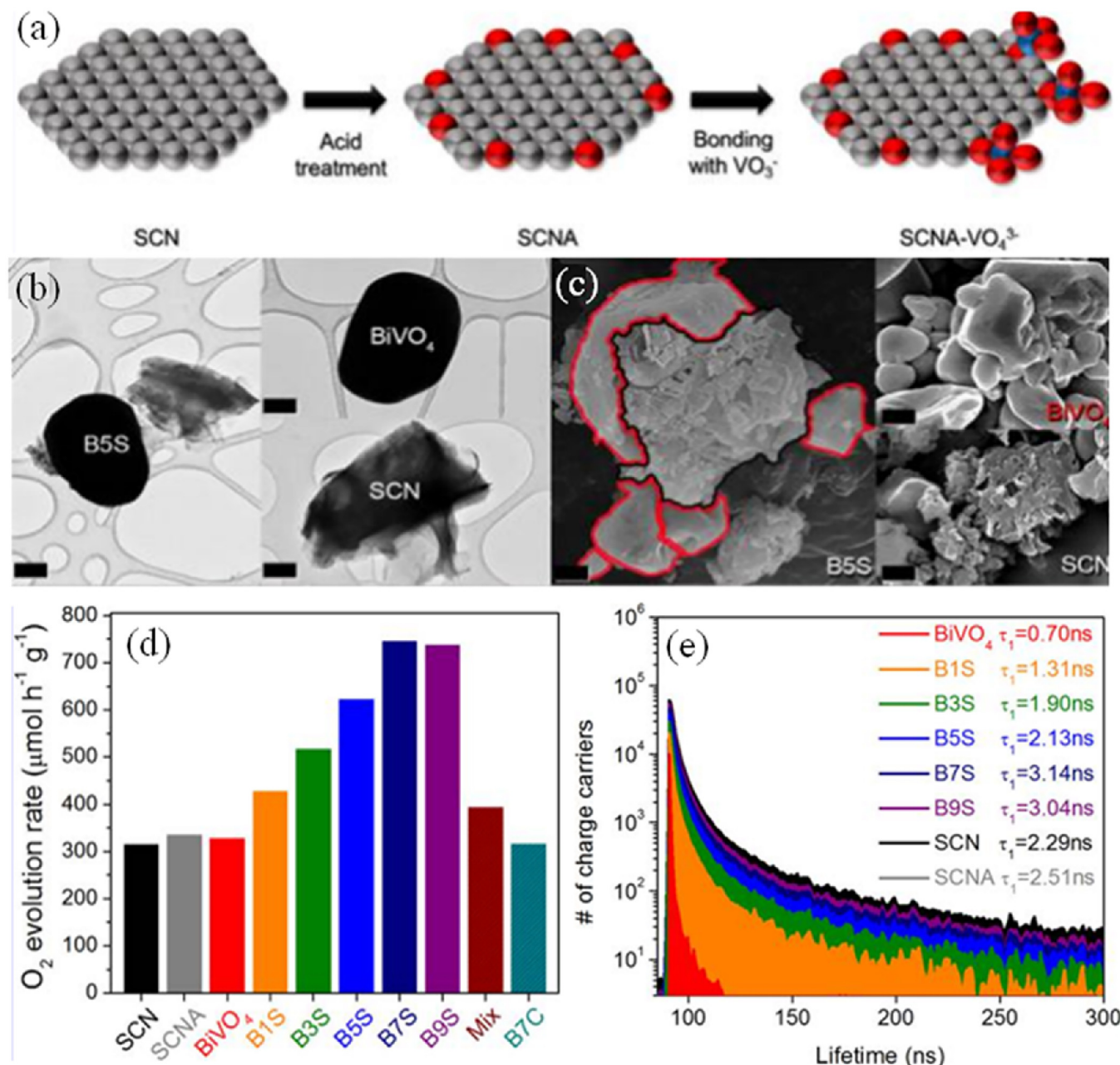


Fig. 10. (a) The Formation of a Composite between SCN and BiVO₄ (gray for SCN red for oxygen, and blue for vanadium atom). (b) TEM and (c) FE-SEM of prepared photocatalysts. (d) Photocatalytic activities of prepared photocatalysts. (e) Charge carrier lifetimes of prepared photocatalysts. Reprinted with permission from ref. [149]. Copyright 2016 American Chemical Society. (For interpretation of the references to colour in this figure legend, the reader is referred to the web version of this article.)

the high photogenerated charges separation efficiency because of the defect sites in Al₂O₃. Additionally, Luo et al. designed CeO₂/P-C₃N₄ photocatalysts by doping phosphorus and coupling with CeO₂ species [157]. The results indicated that the optimum photocatalytic activity of CeO₂/P-C₃N₄ composite was 12.2 times higher than that of pure CeO₂ and 7.9 times than that of pure g-C₃N₄, which was ascribed to the extended the visible light absorption range, enhanced visible light absorption and improved photogenerated charges separation efficiency.

Besides wide-band-gap inorganic semiconductor oxides, other novel semiconductors have been combined with doped g-C₃N₄ for efficient photocatalysis, such as ZnIn₂S₄ [151], BiVO₄ [149], DyVO₄ [158], g-C₃N₄ [159], BiPO₄ [160], Zn_{0.8}Cd_{0.2}S [161], zinc phthalocyanine [146], and so on. Chen et al. fabricated P-C₃N₄/ZnIn₂S₄ nanocomposites by a mixed solvothermal method [151]. The

results indicated that the enhancement of the visible light photocatalytic activity for 4-nitroaniline was resulted from the high separation efficiency of the photoinduced electron–hole pairs on the basis of the construction of a close heterogeneous interface. It is interesting that g-C₃N₄ and B-doped g-C₃N₄ composite semiconductors were fabricated by a facile calcination method [159]. This isotype semiconductors could reduce the recombination of photoinduced electrons and holes, thus enhancing the photocatalytic H₂ evolution activity and improving the degradation efficiency for methyl orange and phenol. In another study, Kong et al. developed composite photocatalysts with bismuth vanadate (BiVO₄) and sulfur-doped graphitic carbon nitride (SCN) by using a one-pot impregnated precipitation method (Fig. 10a) [149]. Sulfur doping can change the band structure by stacking its 2p orbitals on the valence band of pristine g-C₃N₄, thus narrowing the band gap of

$\text{g-C}_3\text{N}_4$ to increase the efficiency [94]. It is observed that the junction between BiVO_4 and SCN is limited to the surface and their inherent bulk morphologies are not changed (Fig. 10b–c). Thus, the catalytic activity of composite photocatalyst for water oxidation ($750 \mu\text{mol h}^{-1} \text{g}^{-1}$) was much enhanced compared to that of pristine BiVO_4 ($328 \mu\text{mol h}^{-1} \text{g}^{-1}$) under identical reaction conditions (Fig. 10d). The enhanced photocatalytic activity can be ascribed to the reduced recombination rate of excited charge carriers by a Z-scheme in the composite photocatalyst, in which excited electrons from BiVO_4 favorably combine to holes in the valence band of $\text{g-C}_3\text{N}_4$. This can be confirmed by the charge carrier lifetime experiment (Fig. 10e). The calculated lifetime (τ_1) of B7S (3.14 ns) is longer than that of SCN (2.29 ns) and BiVO_4 (0.70 ns). Similarly, DyVO_4 has a small band gap ($\sim 2.3 \text{ eV}$) and shows a strong absorption in the visible-light region, which has a matching CB and VB position with $\text{g-C}_3\text{N}_4$. Thus, Li et al. synthesized $\text{DyVO}_4/\text{g-C}_3\text{N}_4\text{I}$ composite semiconductors by a facile heating method [158]. The H_2 evolution rate of the optimal $\text{DyVO}_4/\text{g-C}_3\text{N}_4\text{I}$ composite was 10.6, 4.7 and 1.7 times higher than that of DyVO_4 , $\text{g-C}_3\text{N}_4$ and $\text{g-C}_3\text{N}_4\text{I}$, respectively. The obviously enhanced photoactivity is mainly ascribed to the increased specific surface area, decreased band-gap energy, enhanced absorption in the $400\text{--}700 \text{ nm}$ region and promoted efficient separation of photo-generated carriers.

6. Conclusion and perspectives

Tremendous interest in graphitic carbon nitride as a photocatalyst indicate it emerging as an attractive material in various scientific fields such as photocatalytic organic pollutant degradation, water splitting, CO_2 reduction and organic synthesis, etc. These applications exploit some of the fascinating properties of $\text{g-C}_3\text{N}_4$ which include visible light response, suitable band gap, good redox ability, metal-free nature, environmental friendliness, good chemical and thermal stability, easy fabrication and its polymeric structure allows for easy modifications to alter its properties. However, the pristine $\text{g-C}_3\text{N}_4$ is usually restricted by unsatisfactory photocatalytic efficiency due to the insufficient sunlight absorption, low surface area and the fast recombination of photo-induced electron-hole pairs. Among various modification strategies, element doping is known to be an efficient method to tune the band gap of $\text{g-C}_3\text{N}_4$, which considerably broaden the light responsive range and enhance the charge separation. In this review, recent progress in the development of efficient and low cost doped $\text{g-C}_3\text{N}_4$ systems has been summarized. Typically, metal doping, nonmetal doping, co-doping and heterojunction based on doped $\text{g-C}_3\text{N}_4$ have been explored for the improved photocatalytic activity by increasing the light absorption, improving the charge separation and transportation, enhancing the photocatalytic activity and prolonging the charge carrier lifetime. Generally, the externally doped atoms either substitute for the lattice atoms or exist in the in-planar caves of $\text{g-C}_3\text{N}_4$. Orbital hybridization occurs between the dopant orbital and the molecular orbital of $\text{g-C}_3\text{N}_4$, leading to a tunable electronic structure and potentials of VB and CB. It is anticipated that the element doped $\text{g-C}_3\text{N}_4$ photocatalysts will receive ever increasing research attention in the future.

In summary, metal doping can lead to the formation of new energy levels in the band-gap, extend the spectral response property, and can sometimes reduce the recombination rate of the electron-hole pairs. However, the thermal stability of the doped ions is always poor. Also, the newly created energy bands might act as recombination centres, leading to decreased quantum efficiencies. Nonmetal doping, is an effective strategy to modulate absorbance, redox potentials, and mobility of photo-induced charge carriers. Codoping or tridoping could combine the advantages of these single dopants which exhibits positive influences

on the structural and optical properties, leading to improved photocatalytic performance. Simultaneous doping and heterojunction engineering to modify $\text{g-C}_3\text{N}_4$ with a great possibility for efficient visible-light photocatalysis with high separation rate of the electron-hole pair. In short, elemental doping is one of the appealing strategies to modulate the physicochemical properties of $\text{g-C}_3\text{N}_4$.

Although some encouraging results have been achieved, the development of element doped $\text{g-C}_3\text{N}_4$ in photocatalysis is still at its early stage and there remain many challenges. (1) Modulating the HOMO and LUMO with orientation makes both of them encompasses oxidation and reduction potential for the catalytic reaction while reducing its band gap and enhancing the separation of photo-generated electrons and holes for future improving element doped $\text{g-C}_3\text{N}_4$ photocatalytic efficiency. (2) The origin of element doping-induced visible light absorption, the nature of the chemical states created, and the locations of the dopants are not yet well understood. (3) The mechanisms of photocatalytic enhancement by the element doped $\text{g-C}_3\text{N}_4$ photocatalyst systems are partly unclear. The role and the site of metal ion and heteroatom should be clarified clear. (4) How the defects affect the electronic properties of $\text{g-C}_3\text{N}_4$ and how they can be influenced by doping should be clarified.

In our opinion, there are several directions worthy of attention for element doped $\text{g-C}_3\text{N}_4$ applied in photocatalysis in the future: (1) Codoping or tridoping should be a feasible strategy which could combine the advantages of these single dopants, leading to positive influences on the structural and optical properties. (2) Simultaneous doping and heterojunction engineering could further improve the separation of photogenerated electrons and holes for efficient photocatalytic activity. (3) The combination of element doping and nanostructures fabrication with specific morphologies including nanosheet, mesostructures, nanorods, nanotubes, and nanofibers should be a novel direction. (4) Innovative doping strategy should be developed to modulate the HOMO and LUMO with orientation for high oxidation and reduction potential.

Acknowledgements

The authors gratefully acknowledge the financial support provided by the Foundation for Innovative Research Groups of the National Natural Science Foundation of China (No. 51521006), the Key Project of National Nature Science Foundation of China (No. 71431006), Key research and development project of Hunan Province, China (No. 2016SK2015, No. 2016SK2045), the National Natural Science Foundation of China (No. 51479072, No. 51679082).

References

- [1] X. Yang, Z. Chen, J. Xu, H. Tang, K. Chen, Y. Jiang, Tuning the morphology of $\text{g-C}_3\text{N}_4$ for improvement of Z-Scheme photocatalytic water oxidation, *ACS Appl. Mater. Interfaces* 7 (2015) 15285–15293.
- [2] P. Zhang, J. Zhang, J. Gong, Tantalum-based semiconductors for solar water splitting, *Chem. Soc. Rev.* 43 (2014) 4395.
- [3] Y. Miseki, S. Fujiyoshi, T. Gunji, K. Sayama, Photocatalytic water splitting under visible light utilizing I^3^-/I^- and IO_3^-/I^- redox mediators by Z-scheme system using surface treated PtO_x/WO_3 as O_2 evolution photocatalyst, *Catal. Sci. Technol.* 3 (2013) 1750–1756.
- [4] K. Meyer, M. Ranocchiari, J.a. van Bokhoven, Metal organic frameworks for photo-catalytic water splitting, *Energy Environ. Sci.* 8 (2015) 1923–1937.
- [5] B. Kiss, C. Didier, T. Johnson, T.D. Manning, M.S. Dyer, A.J. Cowan, J.B. Claridge, J.R. Darwent, M.J. Rosseinsky, Photocatalytic water oxidation by a pyrochlore oxide upon irradiation with visible light: rhodium substitution into yttrium titanate, *Angew. Chem.–Int. Ed.* 53 (2014) 14480–14484.
- [6] W. Yu, D. Xu, T. Peng, Enhanced photocatalytic activity of $\text{g-C}_3\text{N}_4$ for selective CO_2 reduction to CH_3OH via facile coupling of ZnO : a direct Z-scheme mechanism, *J. Mater. Chem. A* 0 (2015) 1–12.
- [7] T. Arai, S. Sato, T. Kajino, T. Morikawa, Solar CO_2 reduction using H_2O by a semiconductor/metal-complex hybrid photocatalyst: enhanced efficiency and demonstration of a wireless system using SrTiO_3 photoanodes, *Energy Environ. Sci.* 6 (2013) 1274–1282.

[8] D. Sun, Y. Fu, W. Liu, L. Ye, D. Wang, L. Yang, X. Fu, Z. Li, Studies on photocatalytic CO_2 reduction over $\text{NH}_2\text{-UiO-66}(\text{Zr})$ and its derivatives: towards a better understanding of photocatalysis on metal-organic frameworks, *Chem. Eur. J.* 19 (2013) 14279–14285.

[9] D.H. Lan, H.T. Wang, L. Chen, C.T. Au, S.F. Yin, Phosphorous-modified bulk graphitic carbon nitride: facile preparation and application as an acid-base bifunctional and efficient catalyst for CO_2 cycloaddition with epoxides, *Carbon* 100 (2016) 81–89.

[10] M. Savage, S. Yang, M. Suyetin, E. Bichoutskaia, W. Lewis, A.J. Blake, S.A. Barnett, M. Schröder, A novel bismuth-based metal-organic framework for high volumetric methane and carbon dioxide adsorption, *Chem.—A Eur. J.* 20 (2014) 8024–8029.

[11] H. Wang, X. Yuan, Y. Wu, G. Zeng, X. Chen, L. Leng, H. Li, Synthesis and applications of novel graphitic carbon nitride/metal-organic frameworks mesoporous photocatalyst for dyes removal, *Appl. Catal. B: Environ.* 174–175 (2015) 445–454.

[12] Z. Wu, X. Yuan, H. Wang, Z. Wu, L. Jiang, Facile synthesis of a novel full-spectrum-responsive $\text{Co}_{0.67}\text{S}_4$ nanoparticles for UV-, vis- and NIR-driven photocatalysis, *Appl. Catal. B: Environ.* 202 (2017) 104–111.

[13] H. Wang, X. Yuan, H. Wang, X. Chen, Z. Wu, L. Jiang, W. Xiong, G. Zeng, Facile synthesis of Sb_2S_3 /ultrathin $\text{g-C}_3\text{N}_4$ sheets heterostructures embedded with $\text{g-C}_3\text{N}_4$ quantum dots with enhanced NIR-light photocatalytic performance, *Appl. Catal. B: Environ.* 193 (2016) 36–46.

[14] L. Jiang, X. Yuan, J. Liang, J. Zhang, H. Wang, G. Zeng, Nanostructured core-shell electrode materials for electrochemical capacitors, *J. Power Sources* 331 (2016) 408–425.

[15] Z. Wu, X. Yuan, J. Zhang, H. Wang, L. Jiang, G. Zeng, Photocatalytic decontamination of wastewater containing organic dyes by metal-organic frameworks and their derivatives, *ChemCatChem* (2016) 41–64.

[16] H. Wang, X. Yuan, Y. Wu, G. Zeng, X. Chen, L. Leng, Z. Wu, L. Jiang, H. Li, Facile synthesis of amino-functionalized titanium metal-organic frameworks and their superior visible-light photocatalytic activity for Cr (VI) reduction, *J. Hazard. Mater.* 286 (2015) 187–194.

[17] Y. Liu, X. Yuan, H. Wang, X. Chen, S. Gu, Q. Jiang, Z. Wu, L. Jiang, Y. Wu, G. Zeng, Novel visible light-induced $\text{g-C}_3\text{N}_4\text{-Sb}_2\text{S}_3\text{/Sb}_4\text{O}_5\text{Cl}_2$ composite photocatalysts for efficient degradation of methyl orange, *Catal. Commun.* 70 (2015) 17–20.

[18] Y. Li, X. Yuan, Z. Wu, H. Wang, Z. Xiao, Y. Wu, X. Chen, G. Zeng, Enhancing the sludge dewaterability by electrolysis/electrocoagulation combined with zero-valent iron activated persulfate process, *Chem. Eng. J.* 303 (2016) 636–645.

[19] H. Wang, X. Yuan, Y. Wu, G. Zeng, W. Tu, C. Sheng, Y. Deng, F. Chen, C.J. Wei, Plasmonic Bi nanoparticles and BiOCl sheets as cocatalyst deposited on perovskite-type $\text{ZnSn}(\text{OH})_6$ microparticle with facet-oriented polyhedron for improved visible-light-driven photocatalysis, *Appl. Catal. B Environ.* 209 (2017) 543–553.

[20] J.W. Xu, Z.D. Gao, K. Han, Y. Liu, Y.Y. Song, Synthesis of magnetically separable $\text{Ag}_3\text{PO}_4\text{/TiO}_2\text{/Fe}_3\text{O}_4$ heterostructure with enhanced photocatalytic performance under visible light for photoactivation of bacteria, *ACS Appl. Mater. Interfaces* 6 (2014) 15122–15131.

[21] W. Zhu, P. Liu, S. Xiao, W. Wang, D. Zhang, H. Li, Microwave-assisted synthesis of Ag-doped MOFs-like organotitanium polymer with high activity in visible-light driven photocatalytic NO oxidization, *Appl. Catal. B Environ.* 172–173 (2015) 46–51.

[22] D. Xia, Y. Li, G. Huang, C.C. Fong, T. An, G. Li, H.Y. Yip, H. Zhao, A. Lu, P.K. Wong, Visible-light-driven inactivation of *Escherichia coli* K-12 over thermal treated natural pyrrhotite, *Appl. Catal. B Environ.* 176–177 (2015) 749–756.

[23] H. Huang, H. Zhang, Z. Ma, Y. Liu, H. Ming, H. Li, Z. Kang, Tunable synthesis of metal-graphene complex nanostructures and their catalytic ability for solvent-free cyclohexene oxidation in air, *Nanoscale* 4 (2012) 4964–4967.

[24] D. Mosconi, D. Mazzier, S. Silvestrini, A. Privitera, C. Marega, L. Franco, A. Moretto, Synthesis and photochemical applications of processable polymers enclosing photoluminescent carbon quantum dots, *ACS Nano* 9 (2015) 4156–4164.

[25] G. Ding, W. Wang, T. Jiang, B. Han, H. Fan, G. Yang, Highly selective synthesis of phenol from benzene over a vanadium-doped graphitic carbon nitride catalyst, *ChemCatChem* 5 (2013) 192–200.

[26] M. Xie, X. Dai, S. Meng, X. Fu, S. Chen, Selective oxidation of aromatic alcohols to corresponding aromatic aldehydes using In_2S_3 microsphere catalyst under visible light irradiation, *Chem. Eng. J.* 245 (2014) 107–116.

[27] Z. Zhao, Y. Sun, F. Dong, Graphitic carbon nitride based nanocomposites: a review, *Nanoscale* 7 (2014) 15–37.

[28] A. Fujishima, Electrochemical photolysis of water at a semiconductor electrode, *Nature* 238 (1972) 37–38.

[29] B. Roose, S. Pathak, U. Steiner, Doping of TiO_2 for sensitized solar cells, *Chem. Soc. Rev.* 44 (2015) 8326–8349.

[30] Y. Yao, J. Qin, H. Chen, F. Wei, X. Liu, J. Wang, S. Wang, One-pot approach for synthesis of N-doped $\text{TiO}_2\text{/ZnFe}_2\text{O}_4$ hybrid as an efficient photocatalyst for degradation of aqueous organic pollutants, *J. Hazard. Mater.* 291 (2015) 28–37.

[31] H. Wang, X. Yuan, Y. Wu, G. Zeng, H. Dong, X. Chen, L. Leng, Z. Wu, L. Peng, In situ synthesis of $\text{In}_2\text{S}_3\text{@MIL-125}(\text{Ti})$ core–shell microparticle for the removal of tetracycline from wastewater by integrated adsorption and visible-light-driven photocatalysis, *Appl. Catal. B: Environ.* 186 (2016) 19–29.

[32] L. Zhang, X. Yuan, H. Wang, X. Chen, Z. Wu, Y. Liu, S. Gu, Q. Jiang, G. Zeng, Facile preparation of an $\text{Ag}/\text{AgVO}_3\text{/BiOCl}$ composite and its enhanced photocatalytic behavior for methylene blue degradation, *RSC Adv.* 5 (2015) 98184–98193.

[33] C. Li, P. Zhang, R. Lv, J. Lu, T. Wang, S. Wang, H. Wang, J. Gong, Selective deposition of Ag_3PO_4 on monoclinic $\text{BiVO}_4(040)$ for highly efficient photocatalysis, *Small* 9 (2013) 3951–3956.

[34] P. Zhou, J. Yu, M. Jaroniec, All-solid-state Z-scheme photocatalytic systems, *Adv. Mater.* 26 (2014) 4920–4935.

[35] H. Wang, X. Yuan, Y. Wu, H. Huang, X. Peng, G. Zeng, H. Zhong, J. Liang, M.M. Ren, Graphene-based materials: fabrication, characterization and application for the decontamination of wastewater and wastegas and hydrogen storage/generation, *Adv. Colloid Interface Sci.* 195–196 (2013) 19–40.

[36] W.J. Ong, L.L. Tan, Y.H. Ng, S.T. Yong, S.P. Chai, Graphitic carbon nitride ($\text{g-C}_3\text{N}_4$)-Based photocatalysts for artificial photosynthesis and environmental remediation: are we a step closer to achieving sustainability? *Chem. Rev.* 116 (2016) 7159–7329.

[37] X. Song, J. Hu, H. Zeng, Two-dimensional semiconductors: recent progress and future perspectives, *J. Mater. Chem. C* 1 (2013) 2952.

[38] X. Wang, G. Sun, N. Li, P. Chen, Quantum dots derived from two-dimensional materials and their applications for catalysis and energy, *Chem. Soc. Rev.* 45 (2016) 2239–2262.

[39] G. Mamba, A.K. Mishra, Graphitic carbon nitride ($\text{g-C}_3\text{N}_4$) nanocomposites: a new and exciting generation of visible light driven photocatalysts for environmental pollution remediation, *Appl. Catal. B Environ.* 198 (2016) 347–377.

[40] Z. Wu, H. Zhong, X. Yuan, H. Wang, Adsorptive removal of methylene blue by rhamnolipid-functionalized graphene oxide from wastewater, *Water Res.* 67 (2014) 330–344.

[41] Z. Wu, X. Yuan, H. Zhong, H. Wang, G. Zeng, X. Chen, H. Wang, L. Zhang, J. Shao, Enhanced adsorptive removal of p-nitrophenol from water by aluminum metal-organic framework/reduced graphene oxide composite, *Sci. Rep.* 6 (2016) 25638.

[42] M. Xu, T. Liang, M. Shi, H. Chen, Graphene-like two-dimensional materials, *Chem. Rev.* 113 (2013) 3766–3798.

[43] Y. He, L. Zhang, B. Teng, M. Fan, New application of Z scheme $\text{Ag}_3\text{PO}_4\text{/g-C}_3\text{N}_4$ composite in converting CO_2 to fuel, *Environ. Sci. Technol.* 49 (2015) 649–656.

[44] X. Wang, K. Maeda, A. Thomas, K. Takanabe, G. Xin, J.M. Carlsson, K. Domen, M. Antonietti, A metal-free polymeric photocatalyst for hydrogen production from water under visible light, *Nat. Mater.* 8 (2009) 76–80.

[45] J. Zhu, P. Xiao, H. Li, S.A.C. Carabineiro, Graphitic carbon nitride: synthesis, properties, and applications in catalysis, *ACS Appl. Mater. Interfaces* 6 (2014) 16449–16465.

[46] H. Ou, L. Lin, Y. Zheng, P. Yang, Y. Fang, X. Wang, Tri-s-triazine-based crystalline carbon nitride nanosheets for an improved hydrogen evolution, *Adv. Mater.* (2017) 1700008.

[47] P. Yang, H. Ou, Y. Fang, X. Wang, A facile steam reforming strategy to delaminate layered carbon nitride semiconductors for photoredox catalysis, *Angew. Chem.-Int. Ed.* 56 (2017) 3992–3996.

[48] S. Cao, J. Low, J. Yu, M. Jaroniec, Polymeric photocatalysts based on graphitic carbon nitride, *Adv. Mater.* 27 (2015) 2150–2176.

[49] Y. Tachibana, L. Vayssières, J.R. Durrant, Artificial photosynthesis for solar water-splitting, *Nat. Photonics* 6 (2012) 511–518.

[50] Y. Zhou, L. Zhang, J. Liu, X. Fan, B. Wang, M. Wang, W. Ren, J. Wang, M. Li, J. Shi, Brand new P-doped $\text{g-C}_3\text{N}_4$: enhanced photocatalytic activity for H_2 evolution and Rhodamine B degradation under visible light, *J. Mater. Chem. A* 3 (2015) 3862–3867.

[51] S. Chu, Y. Wang, Y. Guo, J. Feng, C. Wang, W. Luo, X. Fan, Z. Zou, Band structure engineering of carbon nitride: in search of a polymer photocatalyst with high photooxidation property, *ACS Catal.* 3 (2013) 912–919.

[52] L. Shi, L. Liang, F. Wang, M. Liu, S. Zhong, J. Sun, Tetraethylorthosilicate induced preparation of mesoporous graphitic carbon nitride with improved visible light photocatalytic activity, *Catal. Commun.* 59 (2015) 131–135.

[53] Q. Lin, L. Li, S. Liang, M. Liu, J. Bi, L. Wu, Efficient synthesis of monolayer carbon nitride 2D nanosheet with tunable concentration and enhanced visible-light photocatalytic activities, *Appl. Catal. B Environ.* 163 (2015) 135–142.

[54] G. Liao, S. Chen, X. Quan, H. Yu, H. Zhao, Graphene oxide modified $\text{g-C}_3\text{N}_4$ hybrid with enhanced photocatalytic capability under visible light irradiation, *J. Mater. Chem. B* 22 (2012) 2721–2726.

[55] H. Zhao, Y. Dong, P. Jiang, H. Miao, G. Wang, J. Zhang, In situ light-assisted preparation of MoS_2 on graphitic C_3N_4 nanosheets for enhanced photocatalytic H_2 production from water, *J. Mater. Chem. A* 3 (2015) 7375–7381.

[56] J. Fang, H. Fan, Z. Zhu, L. Bing, L. Ma, Dyed graphitic carbon nitride with greatly extended visible-light- responsive range for hydrogen evolution, *J. Catal.* 339 (2016) 93–101.

[57] G. Dong, Y. Zhang, Q. Pan, J. Qiu, A fantastic graphitic carbon nitride ($\text{g-C}_3\text{N}_4$) material: electronic structure, photocatalytic and photoelectronic properties, *J. Photochem. Photobiol. C Photochem. Rev.* 20 (2014) 33–50.

[58] W. Chen, T. Liu, T. Huang, X. Liu, X. Yang, Novel mesoporous P-doped graphitic carbon nitride nanosheets coupled with ZnIn_2S_4 heterostructures with remarkably enhanced, *Nanoscale* (2016) 3711–3719.

[59] C. Xu, Q. Han, Y. Zhao, L. Wang, Y. Li, L. Qu, Sulfur-doped graphitic carbon nitride decorated with graphene quantum dots for an efficient metal-free electrocatalyst, *J. Mater. Chem. A* 3 (2015) 1841–1846.

[60] G. Dong, K. Zhao, L. Zhang, Carbon self-doping induced high electronic conductivity and photoreactivity of g-C₃N₄, *Chem. Commun.* 48 (2012) 6178–6180.

[61] Q. Han, C. Hu, F. Zhao, Z. Zhang, N. Chen, L. Qu, One-step preparation of iodine-doped graphitic carbon nitride nanosheets as efficient photocatalysts for visible light water splitting, *J. Mater. Chem. A* 3 (2015) 4612–4619.

[62] N. Sagara, S. Kamimura, T. Tsubota, T. Ohno, Photoelectrochemical CO₂ reduction by a p-type boron-doped g-C₃N₄ electrode under visible light, *Appl. Catal. B Environ.* 192 (2016) 193–198.

[63] T. Xiong, W. Cen, Y. Zhang, F. Dong, Bridging the g-C₃N₄ interlayers for enhanced photocatalysis, *ACS Catal.* 6 (2016) 2462–2472.

[64] S. Tonda, S. Kumar, S. Kandula, V. Shanker, Fe-doped and –mediated graphitic carbon nitride nanosheets for enhanced photocatalytic performance under natural sunlight, *J. Mater. Chem. A* 2 (2014) 6772.

[65] Z. Li, C. Kong, G. Lu, Visible photocatalytic water splitting and photocatalytic two-Electron oxygen formation over Cu- and Fe-Doped g-C₃N₄, *J. Phys. Chem. C* 120 (2016) 56–63.

[66] J. Ding, L. Wang, Q. Liu, Y. Chai, X. Liu, W.-L. Dai, Remarkable enhancement in visible-light absorption and electron transfer of carbon nitride nanosheets with 1% tungstate dopant, *Appl. Catal. B Environ.* 176–177 (2016) 91–92.

[67] S. Hu, F. Li, Z. Fan, F. Wang, Y. Zhao, Z. Lv, Band gap-tunable potassium doped graphitic carbon nitride with enhanced mineralization ability, *Dalt. Trans.* 44 (2015) 1084–1092.

[68] W. Ong, L. Tan, Y.H., Ng, S., Yong, S., Chai, Graphitic Carbon Nitride (g-C₃N₄)-Based Photocatalysts for Artificial Photosynthesis and Environmental Remediation: Are We A Step Closer To Achieving Sustainability? 116 (2016) 7159–7329.

[69] G. Dong, Y. Zhang, Q. Pan, J. Qiu, A fantastic graphitic carbon nitride (g-C₃N₄) material: electronic structure, photocatalytic and photoelectronic properties, *J. Photochem. Photobiol. C Photochem. Rev.* 20 (2014) 33–50.

[70] X. Wang, S. Blechert, M. Antonietti, Polymeric Graphitic Carbon Nitride for Heterogeneous Photocatalysis, 2 (2012) 1596–1606.

[71] Y. Zheng, L. Lin, B. Wang, X. Wang, Graphitic carbon nitride polymers toward sustainable photoredox catalysis, *Angew. Chem.—Int. Ed.* 54 (2015) 12868–12884.

[72] J. Xu, T.J.K. Brenner, Z. Chen, D. Neher, M. Antonietti, M. Shalom, Upconversion-agent induced improvement of g-C₃N₄ photocatalyst under visible light, *ACS Appl. Mater. Interfaces* 6 (2014) 16481–16486.

[73] M. Zhang, X. Bai, D. Liu, J. Wang, Y. Zhu, Enhanced catalytic activity of potassium-doped graphitic carbon nitride induced by lower valence position, *Appl. Catal. B Environ.* 164 (2015) 77–81.

[74] J. Zhang, S. Hu, Y. Wang, A convenient method to prepare a novel alkali metal sodium doped carbon nitride photocatalyst with a tunable band structure, *RSC Adv.* 4 (2014) 62912–62919.

[75] Y. Wang, Y. Wang, Y. Li, H. Shi, Y. Xu, H. Qin, X. Li, Y. Zuo, S. Kang, L. Cui, Simple synthesis of Zr-doped graphitic carbon nitride towards enhanced photocatalytic performance under simulated solar light irradiation, *Catal. Commun.* 72 (2015) 24–28.

[76] S.W. Hu, L.W. Yang, Y. Tian, X.L. Wei, J.W. Ding, J.X. Zhong, P.K. Chu, Simultaneous nanostructure and heterojunction engineering of graphitic carbon nitride via in situ Ag doping for enhanced photoelectrochemical activity, *Appl. Catal. B Environ.* 163 (2015) 611–622.

[77] Y. Wang, Y. Li, X. Bai, Q. Cai, C. Liu, Y. Zuo, S. Kang, L. Cui, Facile synthesis of Y-doped graphitic carbon nitride with enhanced photocatalytic performance, *Catal. Commun.* 84 (2016) 179–182.

[78] H. Gao, S. Yan, J. Wang, Z. Zou, Ion coordination significantly enhances the photocatalytic activity of graphitic-phase carbon nitride, *Dalton Trans.* 43 (2014) 8178–8183.

[79] H. Pan, Y. Zhang, V.B. Shenoy, H. Gao, Ab initio study on a novel photocatalyst: functionalized graphitic carbon nitride nanotube, *ACS Catal.* 1 (2011) 99–104.

[80] S. Le, T. Jiang, Q. Zhao, X. Liu, Y. Li, B. Fang, M. Gong, Cu-doped mesoporous graphitic carbon nitride for enhanced visible-light driven photocatalysis, *RSC Adv.* 6 (2016) 38811–38819.

[81] B. Yue, Q. Li, H. Iwai, T. Kako, J. Ye, Hydrogen production using zinc-doped carbon nitride catalyst irradiated with visible light, 34401 (2011) 1–8.

[82] Y. Wang, Y. Xu, Y. Wang, H. Qin, X. Li, Y. Zuo, S. Kang, L. Cui, Synthesis of Mo-doped graphitic carbon nitride catalysts and their photocatalytic activity in the reduction of CO₂ with H₂O, *Catal. Commun.* 74 (2016) 75–79.

[83] X. Ye, Y. Cui, X. Qiu, X. Wang, Selective oxidation of benzene to phenol by Fe-CN/TS-1 catalysts under visible light irradiation, *Appl. Catal. B Environ.* 152–153 (2014) 383–389.

[84] X.F. Chen, J.S. Zhang, X.Z. Fu, M. Antonietti, X.C. Wang, Fe-g-C₃N₄-catalyzed oxidation of benzene to phenol using hydrogen peroxide and visible light, *J. Am. Chem. Soc.* 131 (2009) 11658–11659.

[85] L. Zhou, H. Zhang, H. Sun, S. Liu, M.O. Tade, S. Wang, W. Jin, Recent advances in non-metal modification of graphitic carbon nitride for photocatalysis: a historic review, *Catal. Sci. Technol.* 6 (2016) 7002–7023.

[86] X. Song, H. Tao, L. Chen, Y. Sun, Synthesis of Fe/g-C₃N₄ composites with improved visible light photocatalytic activity, *Mater. Lett.* 116 (2014) 265–267.

[87] J. Gao, J. Wang, X. Qian, Y. Dong, H. Xu, R. Song, C. Yan, H. Zhu, Q. Zhong, G. Qian, J. Yao, One-pot synthesis of copper-doped graphitic carbon nitride nanosheet by heating Cu-melamine supramolecular network and its enhanced visible-light-driven photocatalysis, *J. Solid State Chem.* 228 (2015) 60–64.

[88] R. Jin, S. Hu, J. Gui, D. Liu, A convenient method to prepare novel rare earth metal Ce-doped carbon nitride with enhanced photocatalytic activity under visible light, *Bull. Korean Chem. Soc.* 36 (2015) 17–23.

[89] P.-W. Chen, K. Li, Y.-X. Yu, W.-D. Zhang, Cobalt-doped graphitic carbon nitride photocatalysts with high activity for hydrogen evolution, *Appl. Surf. Sci.* 392 (2017) 608–615.

[90] D. Xu, X. Li, J. Liu, L. Huang, Synthesis and photocatalytic performance of europium-doped graphitic carbon nitride, *J. Rare Earths* 31 (2013) 1085–1091.

[91] X. Rong, F. Qiu, J. Rong, X. Zhu, J. Yan, D. Yang, Enhanced visible light photocatalytic activity of W-doped porous g-C₃N₄ and effect of H₂O₂, *Mater. Lett.* 164 (2016) 127–131.

[92] J. Ran, T.Y. Ma, G. Gao, X.-W. Du, S.Z. Qiao, Porous P-doped graphitic carbon nitride nanosheets for synergistically enhanced visible-light photocatalytic H₂ production, *Energy Environ. Sci.* 8 (2015) 3708–3717.

[93] S. Guo, Z. Deng, M. Li, B. Jiang, C. Tian, Q. Pan, H. Fu, Phosphorus-Doped carbon nitride tubes with a layered micro-nanostructure for enhanced visible-Light photocatalytic hydrogen evolution, *Angew. Chem.—Int. Ed.* 55 (2016) 1830–1834.

[94] G. Liu, P. Niu, C. Sun, S.C. Smith, Z. Chen, G.Q. Lu, H.M. Cheng, Unique electronic structure induced high photoreactivity of sulfur-doped graphitic C₃N₄, *J. Am. Chem. Soc.* 132 (2010) 11642–11648.

[95] K. Wang, Q. Li, B. Liu, B. Cheng, W. Ho, J. Yu, Sulfur-doped g-C₃N₄ with enhanced photocatalytic CO₂-reduction performance, *Appl. Catal. B Environ.* 176–177 (2015) 44–52.

[96] C. Lu, P. Zhang, S. Jiang, X. Wu, S. Song, M. Zhu, Z. Lou, Z. Li, F. Liu, Y. Liu, Y. Wang, Z. Le, Photocatalytic reduction elimination of UO₂²⁺ pollutant under visible light with metal-free sulfur doped g-C₃N₄ photocatalyst, *Appl. Catal. B Environ.* 200 (2017) 378–385.

[97] F. He, G. Chen, Y. Yu, Y. Zhou, Y. Zheng, S. Hao, The sulfur-bubble template-mediated synthesis of uniform porous g-C₃N₄ with superior photocatalytic performance, *Chem. Commun.* 51 (2015) 425–427.

[98] Z. Zhao, Y. Sun, F. Dong, Y. Zhang, H. Zhao, Template synthesis of carbon self-doped g-C₃N₄ with enhanced visible to near-infrared absorption and photocatalytic performance, *RSC Adv.* 5 (2015) 39549–39556.

[99] J. Fang, H. Fan, M. Li, C. Long, Nitrogen self-doped graphitic carbon nitride as efficient visible light photocatalyst for hydrogen evolution, *J. Mater. Chem. A* 3 (2015) 13819–13826.

[100] Z.F. Huang, J. Song, L. Pan, Z. Wang, X. Zhang, J.J. Zou, W. Mi, X. Zhang, L. Wang, Carbon nitride with simultaneous porous network and O-doping for efficient solar-energy-driven hydrogen evolution, *Nano Energy* 12 (2015) 646–656.

[101] X. She, L. Liu, H. Ji, Z. Mo, Y. Li, L. Huang, D. Du, H. Xu, H. Li, Template-free synthesis of 2D porous ultrathin nonmetal-doped g-C₃N₄ nanosheets with highly efficient photocatalytic H₂ evolution from water under visible light, *Appl. Catal. B Environ.* 187 (2016) 144–153.

[102] S. Guo, Y. Zhu, Y. Yan, Y. Min, J. Fan, Q. Xu, Holey structured graphitic carbon nitride thin sheets with edge oxygen doping via photo-Fenton reaction with enhanced photocatalytic activity, *Appl. Catal. B Environ.* 185 (2016) 315–321.

[103] C. Lu, R. Chen, X. Wu, M. Fan, Y. Liu, Z. Le, S. Jiang, S. Song, Boron doped g-C₃N₄ with enhanced photocatalytic UO₂²⁺ reduction performance, *Appl. Surf. Sci.* 360 (2016) 1016–1022.

[104] G. Zhang, M. Zhang, X. Ye, X. Qiu, S. Lin, X. Wang, Iodine modified carbon nitride semiconductors as visible light photocatalysts for hydrogen evolution, *Adv. Mater.* 26 (2014) 805–809.

[105] Z.A. Lan, G. Zhang, X. Wang, A facile synthesis of Br-modified g-C₃N₄ semiconductors for photoredox water splitting, *Appl. Catal. B Environ.* 192 (2016) 116–125.

[106] Y. Wang, Y. Di, M. Antonietti, H. Li, X. Chen, X. Wang, Excellent visible-light photocatalysis of fluorinated polymeric carbon nitride solids, *Chem. Mater.* 22 (2010) 5119–5121.

[107] Y. Zhang, T. Mori, J. Ye, M. Antonietti, Phosphorus-doped carbon nitride solid: enhanced electrical conductivity and photocurrent generation, *J. Am. Chem. Soc.* 132 (2010) 6294–6295.

[108] L. Zhang, X. Chen, J. Guan, Y. Jiang, T. Hou, X. Mu, Facile synthesis of phosphorus doped graphitic carbon nitride polymers with enhanced visible-light photocatalytic activity, *Mater. Res. Bull.* 48 (2013) 3485–3491.

[109] S.Z. Hu, L. Ma, J.G. You, F.Y. Li, Z.P. Fan, F. Wang, D. Liu, J.Z. Gui, A simple and efficient method to prepare a phosphorus modified g-C₃N₄ visible light photocatalyst, *RSC Adv.* 4 (2014) 21657–21663.

[110] Y. Deng, L. Tang, G. Zeng, Z. Zhu, M. Yan, Y. Zhou, J. Wang, Y. Liu, J. Wang, Insight into highly efficient simultaneous photocatalytic removal of Cr(VI) and 2,4-dichlorophenol under visible light irradiation by phosphorus doped porous ultrathin g-C₃N₄ nanosheets from aqueous media: performance and reaction mechanism, *Appl. Catal. B Environ.* 203 (2017) 343–354.

[111] Y.P. Zhu, T.Z. Ren, Z.Y. Yuan, Mesoporous phosphorus-doped g-C₃N₄ nanostructured flowers with superior photocatalytic hydrogen evolution performance, *ACS Appl. Mater. Interfaces* 7 (2015) 16850–16856.

[112] B. Chai, J. Yan, C. Wang, Z. Ren, Y. Zhu, Enhanced visible light photocatalytic degradation of Rhodamine B over phosphorus doped graphitic carbon nitride, *Appl. Surf. Sci.* (2016) 4–11.

[113] T.Y. Ma, J. Ran, S. Dai, M. Jaroniec, S.Z. Qiao, Phosphorus-doped graphitic carbon nitrides grown in situ on carbon-fiber paper: flexible and reversible oxygen electrodes, *Angew. Chem.–Int. Ed.* 54 (2015) 4646–4650.

[114] T.Y. Ma, S. Dai, M. Jaroniec, S.Z. Qiao, Graphitic carbon nitride nanosheet–carbon nanotube three-dimensional porous composites as high-performance oxygen evolution electrocatalysts, *Angew. Chem.–Int. Ed.* 53 (2014) 7281–7285.

[115] X. She, H. Xu, Y. Xu, J. Yan, J. Xia, L. Xu, Y. Song, Y. Jiang, Q. Zhang, H. Li, Exfoliated graphene-like carbon nitride in organic solvents: enhanced photocatalytic activity and highly selective and sensitive sensor for the detection of trace amounts of Cu^{2+} , *J. Mater. Chem. A* 2 (2014) 2563.

[116] H. Xu, J. Yan, X. She, L. Xu, J. Xia, Y. Xu, Y. Song, L. Huang, H. Li, Graphene-analogue carbon nitride: novel exfoliation synthesis and its application in photocatalysis and photoelectrochemical selective detection of trace amount of Cu^{2+} , *Nanoscale* 6 (2014) 1406–1415.

[117] H. Yaghoubi, Z. Li, Y. Chen, H.T. Ngo, V.R. Bhethanabotla, B. Joseph, S. Ma, R. Schlaif, A. Takshi, Toward a visible light-driven photocatalyst: the effect of midgap-states-induced energy gap of undoped TiO_2 nanoparticles, *ACS Catal.* 5 (2015) 327–335.

[118] S. Lin, X. Ye, X. Gao, J. Huang, Mechanistic insight into the water photooxidation on pure and sulfur-doped $\text{g-C}_3\text{N}_4$ photocatalysts from DFT calculations with dispersion corrections, *J. Mol. Catal. A Chem.* 406 (2015) 137–144.

[119] Q. Fan, J. Liu, Y. Yu, S. Zuo, B. Li, A simple fabrication for sulfur doped graphitic carbon nitride porous rods with excellent photocatalytic activity degrading RhB dye, *Appl. Surf. Sci.* 391 (2016) 360–368.

[120] J. Hong, X. Xia, Y. Wang, R. Xu, Mesoporous carbon nitride with in situ sulfur doping for enhanced photocatalytic hydrogen evolution from water under visible light, *J. Mater. Chem. 22* (2012) 15006–15012.

[121] L.L. Feng, Y. Zou, C. Li, S. Gao, L.J. Zhou, Q. Sun, M. Fan, H. Wang, D. Wang, G.D. Li, X. Zou, Nanoporous sulfur-doped graphitic carbon nitride microrods: a durable catalyst for visible-light-driven H_2 evolution, *Int. J. Hydrogen Energy* 39 (2014) 15373–15379.

[122] L. Cao, R. Wang, D. Wang, Synthesis and characterization of sulfur self-doped $\text{g-C}_3\text{N}_4$ with efficient visible-light photocatalytic activity, *Mater. Lett.* 149 (2015) 50–53.

[123] X. Ma, Y. Lv, J. Xu, Y. Liu, R. Zhang, Y. Zhu, A strategy of enhancing the photoactivity of $\text{g-C}_3\text{N}_4$ via doping of nonmetal elements: a first-principles study, *J. Phys. Chem. C* 116 (2012) 23485–23493.

[124] J. Li, B. Shen, Z. Hong, B. Lin, B. Gao, Y.-L. Chen, A facile approach to synthesize novel oxygen-doped $\text{g-C}_3\text{N}_4$ with superior visible-light photoreactivity, *Chem. Commun.* 4 (2012) 1–9.

[125] S. Yang, Y. Gong, J. Zhang, L. Zhan, L. Ma, Z. Fang, R. Vajtai, X. Wang, P.M. Ajayan, Exfoliated graphitic carbon nitride nanosheets as efficient catalysts for hydrogen evolution under visible light, *Adv. Mater.* 25 (2013) 2452–2456.

[126] P. Niu, L. Zhang, G. Liu, H.M. Cheng, Graphene-like carbon nitride nanosheets for improved photocatalytic activities, *Adv. Funct. Mater.* 22 (2012) 4763–4770.

[127] Y. Li, S. Wu, L. Huang, J. Wang, H. Xu, H. Li, Synthesis of carbon-doped $\text{g-C}_3\text{N}_4$ composites with enhanced visible-light photocatalytic activity, *Mater. Lett.* 137 (2014) 281–284.

[128] P. Zhang, X. Li, C. Shao, Y. Liu, Hydrothermal synthesis of carbon-rich graphitic carbon nitride nanosheets for photoredox catalysis, *J. Mater. Chem. A* 3 (2015) 3281–3284.

[129] S.C. Yan, Z.S. Li, Z.G. Zou, Photodegradation of rhodamine B and methyl orange over boron-doped $\text{g-C}_3\text{N}_4$ under visible light irradiation, *Langmuir* 26 (2010) 3894–3901.

[130] Z. Lin, X. Wang, Nanostructure engineering and doping of conjugated carbon nitride semiconductors for hydrogen photosynthesis, *Angew. Chem.–Int. Ed.* 52 (2013) 1735–1738.

[131] L. Ge, C. Han, X. Xiao, L. Guo, Y. Li, Enhanced visible light photocatalytic hydrogen evolution of sulfur-doped polymeric $\text{g-C}_3\text{N}_4$ photocatalysts, *Mater. Res. Bull.* 48 (2013) 3919–3925.

[132] J. Chen, Z. Hong, Y. Chen, B. Lin, B. Gao, One-step synthesis of sulfur-doped and nitrogen-deficient $\text{g-C}_3\text{N}_4$ photocatalyst for enhanced hydrogen evolution under visible light, *Mater. Lett.* 145 (2015) 129–132.

[133] M. Nasir, S. Bagwasi, Y. Jiao, F. Chen, B. Tian, J. Zhang, Characterization and activity of the Ce and N co-doped TiO_2 prepared through hydrothermal method, *Chem. Eng. J.* 236 (2014) 388–397.

[134] X. Shen, Z. Liu, S. Xie, J. Guo, Degradation of nitrobenzene using titania photocatalyst co-doped with nitrogen and cerium under visible light illumination, 162 (2009) 1193–1198.

[135] C. Fu, Y. Gong, Y. Wu, J. Liu, Z. Zhang, C. Li, L. Niu, Photocatalytic enhancement of TiO_2 by B and Zr co-doping and modulation of microstructure, *Appl. Surf. Sci.* 379 (2016) 83–90.

[136] J. Zhao, L. Ma, H. Wang, Y. Zhao, J. Zhang, S. Hu, Novel band gap-tunable K-Na co-doped graphitic carbon nitride prepared by molten salt method, *Appl. Surf. Sci.* 332 (2015) 625–630.

[137] S. Hu, L. Ma, J. You, F. Li, Z. Fan, G. Lu, D. Liu, J. Gui, Enhanced visible light photocatalytic performance of $\text{g-C}_3\text{N}_4$ photocatalysts co-doped with iron and phosphorus, *Appl. Surf. Sci.* 311 (2014) 164–171.

[138] S. Zhang, J. Li, M. Zeng, J. Li, J. Xu, X. Wang, Bandgap engineering and mechanism study of nonmetal and metal ion codoped carbon nitride: C+Fe as an example, *Chem.–A Eur. J.* 20 (2014) 9805–9812.

[139] H. Ma, Y. Li, S. Li, N. Liu, Novel PO codoped $\text{g-C}_3\text{N}_4$ with large specific surface area: hydrothermal synthesis assisted by dissolution?precipitation process and their visible light activity under anoxic conditions, *Appl. Surf. Sci.* 357 (2015) 131–138.

[140] Z. Lin, X. Wang, Ionic liquid promoted synthesis of conjugated carbon nitride photocatalysts from urea, *ChemSusChem* 7 (2014) 1547–1550.

[141] H.Q. Ma, S. Zhao, S. Li, N. Liu, A facile approach to synthesizing S-Co-O tridoped $\text{g-C}_3\text{N}_4$ with enhanced oxygen-free photocatalytic performance via a hydrothermal post-treatment, *RSC Adv.* 5 (2015) 79585–79592.

[142] S. Hu, L. Ma, Y. Xie, F. Li, Z. Fan, F. Wang, Q. Wang, Y. Wang, X. Kang, G. Wu, Hydrothermal synthesis of oxygen functionalized S-P codoped $\text{g-C}_3\text{N}_4$ nanorods with outstanding visible light activity under anoxic conditions, *Dalt. Trans.* 44 (2015) 20889–20897.

[143] J. Zhang, Y. Wu, M. Xing, S. Ahmed, K. Leghari, S. Sajjad, Development of modified N doped TiO_2 photocatalyst with metals, nonmetals and metal oxides, (2010) 715–726.

[144] S. Hu, J. Zhu, L. Wu, X. Wang, P. Liu, Y. Zhang, Z. Li, Effect of fluorination on photocatalytic degradation of rhodamine B over $\text{In(OH)}_3\text{S}_2$: promotion or suppression? *J. Phys. Chem. C* 115 (2011) 460–467.

[145] J. Zhang, M. Zhang, R.Q. Sun, X. Wang, A facile band alignment of polymeric carbon nitride semiconductors to construct isotype heterojunctions, *Angew. Chem.–Int. Ed.* 51 (2012) 10145–10149.

[146] Q. Liang, M. Zhang, C. Liu, S. Xu, Z. Li, Sulfur-doped graphitic carbon nitride decorated with zinc phthalocyanines towards highly stable and efficient photocatalysis, *Appl. Catal. A Gen.* 519 (2016) 107–115.

[147] J.Y. Su, P. Geng, X.Y. Li, Q.D. Zhao, X. Quan, G.H. Chen, Novel phosphorus doped carbon nitride modified TiO_2 nanotube arrays with improved photoelectrochemical performance, *Nanoscale* 7 (2015) 16282–16289.

[148] F. Raziq, Y. Qu, X. Zhang, M. Humayun, J. Wu, A. Zada, H. Yu, X. Sun, L. Jing, Enhanced cocatalyst-Free visible-Light activities for photocatalytic fuel production of $\text{g-C}_3\text{N}_4$ by trapping holes and transferring electrons, *J. Phys. Chem. C* 120 (2016) 98–107.

[149] H.J. Kong, D.H. Won, J. Kim, S.I. Woo, Sulfur doped $\text{g-C}_3\text{N}_4/\text{BiVO}_4$ composite photocatalyst for water oxidation under visible light, *Chem. Mater.* 28 (2016) 1318–1324.

[150] L. Ye, D. Wang, S. Chen, Fabrication and enhanced photoelectrochemical performance of MoS_2/S -Doped $\text{g-C}_3\text{N}_4$ heterojunction film, *ACS Appl. Mater. Interfaces* 8 (2016) 5280–5289.

[151] W. Chen, T.-Y. Liu, T. Huang, X. Liu, X. Yang, Novel mesoporous P-doped graphitic carbon nitride nanosheets coupled with ZnIn_2S_4 nanosheets as efficient visible light driven heterostructures with remarkably enhanced photo-reduction activity, *Nanoscale* 8 (2016) 3711–3719.

[152] H. Park, Y. Park, W. Kim, W. Choi, Surface modification of TiO_2 photocatalyst for environmental applications, *J. Photochem. Photobiol. C Photochem. Rev.* 15 (2013) 1–20.

[153] T. Ochiai, A. Fujishima, Photoelectrochemical properties of TiO_2 photocatalyst and its applications for environmental purification, *J. Photochem. Photobiol. C Photochem. Rev.* 13 (2012) 247–262.

[154] K. Nakata, A. Fujishima, TiO_2 photocatalysis: design and applications, *J. Photochem. Photobiol. C Photochem. Rev.* 13 (2012) 169–189.

[155] Y. Bu, Z. Chen, Effect of oxygen-doped C_3N_4 on the separation capability of the photoinduced electron-hole pairs generated by $\text{O-C}_3\text{N}_4@{\text{TiO}}_2$ with quasi-shell-core nanostructure, *Electrochim. Acta* 144 (2014) 42–49.

[156] Y. Wang, Y. Zeng, B. Li, A. Li, P. Yang, L. Yang, G. Wang, J. Chen, R. Wang, In-situ hydrothermal synthesized $\gamma\text{-Al}_2\text{O}_3/\text{O-g-C}_3\text{N}_4$ heterojunctions with enhanced visible-light photocatalytic activity in water splitting for hydrogen, *J. Energy Chem.* 25 (2016) 594–600.

[157] J. Luo, X. Zhou, L. Ma, X. Xu, Enhancing visible-light photocatalytic activity of $\text{g-C}_3\text{N}_4$ by doping phosphorus and coupling with CeO_2 for the degradation of methyl orange under visible light irradiation, *RSC Adv.* 5 (2015) 68728–68735.

[158] H. Li, Y. Liu, Y. Cui, W. Zhang, C. Fu, X. Wang, Facile synthesis and enhanced visible-light photoactivity of $\text{DyVO}_4/\text{g-C}_3\text{N}_4$ composite semiconductors, *Appl. Catal. B Environ.* 183 (2016) 426–432.

[159] H. Li, Y. Liu, X. Gao, C. Fu, X. Wang, Facile synthesis and enhanced visible-light photocatalysis of graphitic carbon nitride composite semiconductors, *ChemSusChem* 8 (2015) 1189–1196.

[160] J. Yuan, Q. Gao, X. Li, Y. Liu, Y. Fang, S. Yang, F. Peng, X. Zhou, Novel 3-D nanoporous graphitic C_3N_4 nanosheets with heterostructured modification for efficient visible-light photocatalytic hydrogen production, *RSC Adv.* 4 (2014) 52332–52337.

[161] W. Tian, N. Li, J. Zhou, A novel P-doped $\text{g-C}_3\text{N}_4/\text{Zn}_{0.8}\text{Cd}_{0.2}\text{S}$ composite photocatalyst for degradation of methylene blue under simulated sunlight, *Appl. Surf. Sci.* 361 (2016) 251–258.